

Article

The Secondary Minerals from the Pillow Basalt of Salsette-Mumbai, Deccan Volcanic Province, India

Berthold Ottens ^{1,*}, Ralf Schuster ² and Zsolt Benkó ³¹ Independent Researcher, Krackhardtstr. 4, D-96047 Bamberg, Germany² Geologische Bundesanstalt, Neulinggasse 38, A-1030 Vienna, Austria; ralf.schuster@geologie.ac.at³ Institute for Nuclear Research, Hungarian Academy of Sciences, Bem tér 18/C, H-4026 Debrecen, Hungary; benko.zsolt@atomki.hu

* Correspondence: ottens-mineralien@t-online.de; Tel.: +49-951-70023280

Abstract: Secondary minerals occur within the tholeiitic basalts of Salsette Island in the greater Mumbai region, as well as in other localities in the Deccan Volcanic Province (DVP). However, the secondary minerals of Salsette Island show remarkable differences with respect to their mineral speciation and precipitation sequence, which are both due to their unique geological environment. The greater Mumbai region is built up by the Salsette subgroup, which represents the youngest sequence of the DVP. It formed subsequently to the main phase of DVP activity in Danian time (62.5 to 61.5 Ma), in the course of the India–Laxmi Ridge–Seychelles breakup. The main part of the Salsette subgroup consists of tholeiitic basaltic flows with pillows, pillow breccia, and hyaloclastite, which formed in contact with brackish and fresh water in a lagoonal environment. In some places, intertrappeans are represented by fossiliferous shallow water sediments. On the top, trachytic and rhyolitic subaqueous volcanoclastics occur, and some dioritic bodies have intruded nearby. Due to differing fluid rock interactions, several distinctly different secondary minerals developed in the void spaces of the hyaloclastite breccia of the interpillow matrix and in the pillow cavities. The highly permeable hyaloclastite breccia formed an open system, where pronounced precipitation occurred in the early phase and at higher temperatures. In contrast, the pillow cavities were a temporally closed system and contained, for example, more low-temperature zeolites. The genesis of the secondary minerals can be summarized as follows: During initial cooling of the volcanic rocks at about 62 Ma, the first mineralization sequence developed with chlorite, laumontite I, quartz, and calcite I. Ongoing magmatic activity caused reheating and the main phase of precipitation at prehnite–pumpellyite facies conditions. During generally decreasing temperatures, in the range of 270–180 °C, babingtonite, laumontite II, prehnite, julgoldite, yugawaralite, calcite II, ilvaite, pumpellyite, and gryolite developed. The fluid contained SiO₂ + Al₂O₃ + FeO + MgO + CaO, and minor MnO and Na₂O, and was predominately mineralized by the decomposition of basaltic glass. Further temperature decreases caused zeolite facies conditions and precipitation of okenite I, scolecite, heulandite, stilbite, and finally chabazite I, in the temperature range of 180 °C to less than 100 °C. As FeO, MgO, and MnO were then absent, an interaction of the fluid with plagioclase is indicated. According to Rb–Sr and K–Ar ages on apophyllite–K, a third phase of precipitation with apophyllite–K, okenite II, and chabazite II occurred in the late Eocene to early Oligocene (30–40 Ma). The new hydrothermal fluid additionally contained K₂O, and temperatures of 50–100 °C can be expected.

Keywords: Deccan Volcanic Province; secondary minerals; zeolites; prehnite–pumpellyite facies; geochronology



Citation: Ottens, B.; Schuster, R.; Benkó, Z. The Secondary Minerals from the Pillow Basalt of Salsette-Mumbai, Deccan Volcanic Province, India. *Minerals* **2022**, *12*, 444. <https://doi.org/10.3390/min12040444>

Academic Editors: Nikolaos Kantiranis and Anestis A. Filippidis

Received: 15 March 2022

Accepted: 31 March 2022

Published: 4 April 2022

Publisher's Note: MDPI stays neutral with regard to jurisdictional claims in published maps and institutional affiliations.



Copyright: © 2022 by the authors. Licensee MDPI, Basel, Switzerland. This article is an open access article distributed under the terms and conditions of the Creative Commons Attribution (CC BY) license (<https://creativecommons.org/licenses/by/4.0/>).

1. Introduction

The Deccan Volcanic Province (DVP) is one of the largest igneous provinces on Earth. During recent decades, the genesis, composition, stratigraphy, and timing of eruption of the DVP flood basalts, including the greater Mumbai area, have been studied extensively

(e.g., [1–6]). One conspicuous feature of the Deccan basalts is the frequent occurrence of secondary minerals (e.g., zeolites, carbonates, silicates) in vesicles and cavities of the rocks, which often form large, euhedral crystals [7,8]. The precipitation of such secondary minerals is commonly explained by low grade metamorphic reactions in different P/T zones during initial cooling, burial [1,9,10], or in the context of hydrothermal events [11]. Early studies on secondary minerals of the DVP favored the hypothesis of formation in different burial zones [1,8]. However, later investigations by Jeffery [12] and Sabale and Vishwakarma [13] refuted this hypothesis, based on better knowledge about the distribution of the secondary minerals and their relation to the stratigraphy and former overburden.

The main Deccan Volcanic Province (DVP) consists of tholeiitic basalts occurring as sheet-like flows formed under terrestrial conditions. The variation of the mineral assemblages in the cavities therein is limited. Recently, Ottens et al. [14] developed a mineralization model for Savda/Jalgaon in the main DVP and concluded with a multi-stage model that included burial metamorphism and postvolcanic hydrothermal activity. In contrast, the basalts in the Mumbai (formerly Bombay) region erupted in a lagoonal to shallow marine environment, forming pillows and volcanoclastics [15–17]. The mineral association appearing in these cavities shows some remarkable differences with respect to those in that area of the main DVP, which consist predominantly of lobate flows. This was first mentioned by Sukheswala et al. [8], and the first detailed descriptions of the secondary minerals from Salsette Island were reported by Ottens [18,19]. The most delicate secondary minerals were found in certain quarries, which operated until 1997. After that, they were overbuilt by houses and new findings were only made very rarely during building foundation works.

The target of this study is to describe the secondary minerals in the pillows and interpillow matrix at Salsette Island and their genesis in a unique geological environment. The study includes field observations from quarries over a time span ranging from 1980 until 1999. Further data on the chemical composition of some secondary minerals, and on the crystallization age of apophyllite, are also reported on. These data allow the determination of the secondary minerals' precipitation sequence and discussion of their formation environment. Finally, the data on the secondary minerals within the cavities of the Salsette spilite are compared to those of the main DVP.

2. Geological Setting and Mineralization

The DVP formed 67.5 to 60.5 Ma ago and covers an area of about 500,000 km² in western and central India (e.g., [3,20,21]). The main part of the tholeiitic flood basalt extruded from certain fissure systems [5,6] within just one million years between 65.4 to 66.4 Ma, before and after the Cretaceous–Paleogene boundary [5,22,23]. This main phase was followed by rifting during the course of the India–Laxmi Ridge–Seychelles breakup at 62.5 Ma. This rifting was also accompanied by magmatism, which occurred during the syn-breakup and continued post-breakup, up to 60.5 Ma in the Mumbai area and the Seychelles [24,25]. With respect to rift related structures, the main DVP can be subdivided into areas east or west of the north–south trending, extensional Panvel flexure zone.

The DVP east of the Panvel flexure is formed by subhorizontal, 1° to 2° east-dipping monotonous and successive tholeiitic lava flows, which were extruded during the main phase of volcanic activity. Based on their typical surface morphology, both lobate and sheet flows can be distinguished [26,27]. The units of lobate flow are vesicular with pipe amygdalae at the base and they are strongly vesicular at the top, with spherical vesicles and a rather dense core zone. Individual flows consist of a number of sheet-like emplaced cooling units and ellipsoidal toes. They formed subaerially in a terrestrial environment and are characterized by weathering profiles and bole horizons without fossilized intertrappeans; if boles are mentioned [5,28]. Based on extensive geochemical stratigraphic work in the Western Ghats, the main part of the DVP volcanic sequence has been divided into three subgroups and eleven formations, with a total stratigraphic thickness of about 3.4 km [6,27]. The part of the DVP west of the Panvel flexure is dipping

towards the west by up to 25° [15,29,30] and is characterized by a domino-type block-faulted structure [6].

In the greater Mumbai area (including the Salsette, Madh, Gorai, Trombay, and Mumbai islands), the subgroups exposed in the Western Ghats are overlain by the Salsette subgroup [6,16], which formed during the last phase of volcanic activity [31] at 62 to 60.5 Ma [6,32]. This area shows remarkable differences with respect to the units below. The Salsette subgroup contains not only basalt, but also trachyte and rhyolite, as well as felsic and basic tuffs. They partially erupted subaqueously near a paleo coast line, forming pillowed flows and layers of hyaloclastite and explosive volcanic breccia [16,17,31]. In the Salsette subgroup formations of southern Mumbai, seven individual flows were identified, separated by 2 to 5 m thick sedimentary intertrappeans. The succession formed in a lagoonal setting and, according to the variety of fossils, in a brackish or even freshwater environment [33–35].

Salsette Island is characterized by a range of hills extending north–south along its center (Figure 1). Amygdaloidal tholeiitic basalt occupies most of the eastern part of the island, whereas spilitic basalt with pillow structure is widespread on the western slopes of the hills (Figure 2a). At several places, the basalt was quarried as a construction material until 1997. The most important quarries were (1) Dahisar, (19°15' N, 72°52' E; 30–130 m asl); (2) Damupada, (19°12' N, 72°52' E; 55–65 m asl); (3) Kurar, (19°11' N, 72°52' E; 20–40 m asl); (4) Pathanwadi (19°10' N, 72°52' E; 30–50 m asl); and (5) Amboli (19°08' N, 72°50' E). The Kurar quarry was also denoted as the Kurad, Khandivali, or Malad quarry. Due to heavy urbanization, most of the natural outcrops and quarries in the Mumbai area have, regrettably, been destroyed, or are at least, highly inaccessible. The Dahisar River bed pillows are located at 19°13' N, 72°53' E.

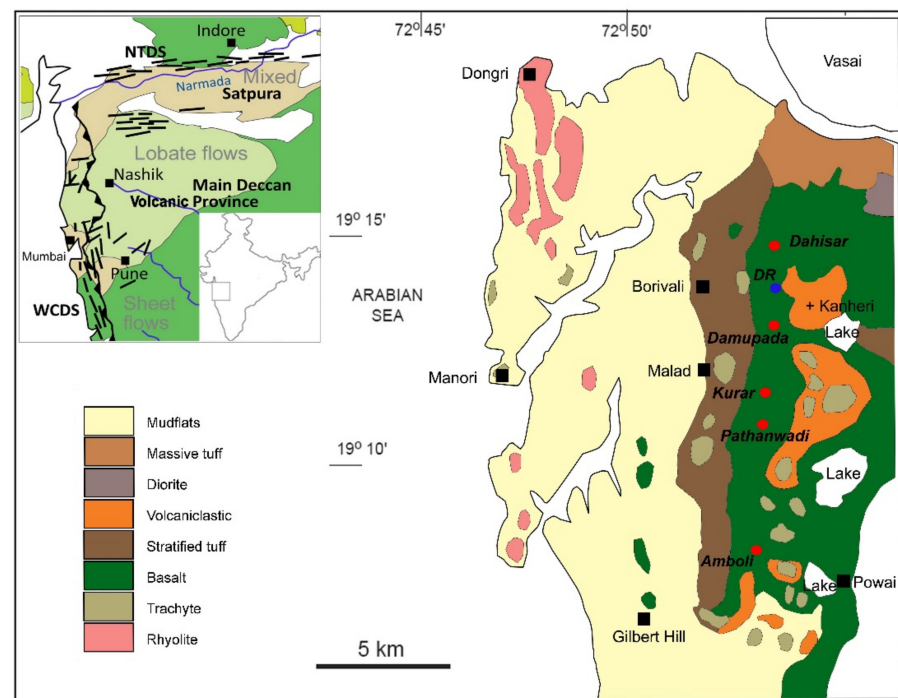


Figure 1. Geological map of Salsette Island, Mumbai (modified after Sheth et al. [31], with the position of the investigated quarries (red dots) and the Dahisar river bed pillows (blue dot and DR, respectively).

The studied quarries on the Salsette Islands are situated in the pillowed basalts with variable degrees of spilitic alteration (Figure 2a). They probably belong to the Sewri formation [16,17]. However, Cripps et al. [35] argued that the flow-types are not geochemically related to the Sewri formation and were coeval with terminal Wai subgroup eruptions occurring along the Western Ghats. Intertrappeans, such as those on the southern Mumbai Island, were not observed. Duraiswami et al. [17] studied the rock formations between the

Borivali and Kanheri caves in the Sanjay Gandhi National Park on Salsette Island. They identified a sequence with a subaqueous emplaced flow with pillow structure, followed by overlying subaqueously erupted explosive volcanoclastics. Remarkable exposures of pillow basalt are also present in the Dahisar river bed (Figure 2b). It is likely that the pillow basalts in the quarries belong to the same pillow flow as those in the Dahisar river bed.

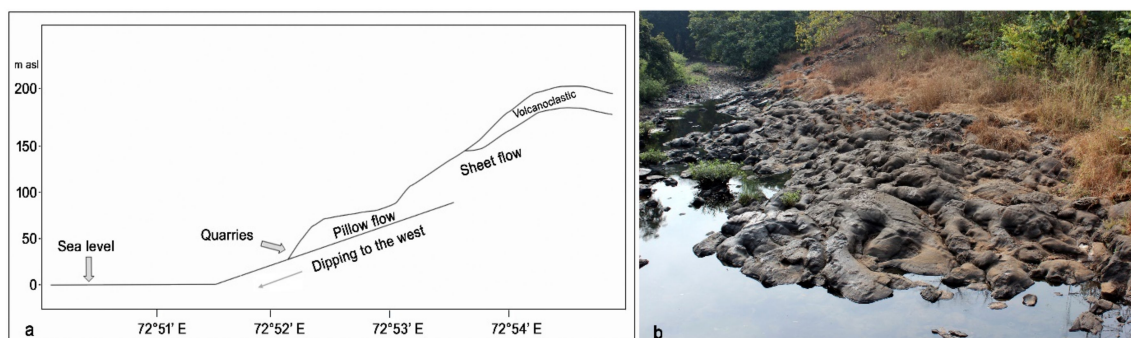


Figure 2. (a) Schematic illustration of an east–west section between an imaginary north–south line of the quarries and the Kanheri caves, displaying the position of the quarries and the Dahisar river bed pillow basalts. The pillow basalts and sheet lava are overlain locally by volcanoclastics. (b) Oblong entities of a pillow flow in the Dahisar river bed. The stream bed is ~15 m wide.

The first comprehensive studies on zeolites and associated secondary minerals from the Deccan Traps of Western India were published by Sukheswala et al. [7,8]. Their reports included remarks on a few minerals, such as laumontite, prehnite, okenite, and gyrolite, from some specific outcrops of greater Mumbai. The comprehensive report about the secondary minerals from the main DVP given by Wilke [36] also contains information on minerals from greater Mumbai, but it lacks a discussion of their relation to the volcanic host rocks. Studies focused on the secondary minerals from Greater Mumbai include the following papers: Yugawaralite, a rare zeolite, was first described in detail by Wise [37]. Meyer [38] studied the chemical composition of gyrolite and described the correlation between its color and its Fe and Mn content. Furthermore, Wise and Moller [39] examined Ca-Fe-silicates and zeolites from the basalt cavities in Salsette Island. A first report specifically on the whole sequence of secondary minerals was published by Ottens [19]. However, a complete description of the secondary minerals from the Salsette Island, concerning their precipitation sequence and genesis within partly spilitized pillow basalt and hyaloclastite, respectively, is as of yet not available.

3. Materials and Methods

3.1. Sample Material

The investigated material includes dozens of hand specimens of secondary minerals. These specimens come from cavities within pillows and from the void spaces in between, and were collected from the Dahisar, Damupada, Kurar, Pathanwadi, and Amboli quarries (Figure 1), between 1980 and 1999.

3.2. Analytical Methods

Thin sections from the basaltic host rock were investigated under a petrographic microscope, and rock slabs were measured using a scanning electron microscope (SEM-EDX).

Several mineral samples were identified by X-ray diffraction analysis (XRD). The mineralogical compositions of the separated and prepared (<20 µm) fractions were analyzed by X-ray diffraction using a URD 6 (Seifert/Freiburger Präzisionsmechanik, Freiberg, Germany) with Co K_α radiation in the range 5–80° (2θ). Analytical conditions included a detector slit of 0.25 mm, 0.03-µm step width, and a 5-s measuring time. The data were then

evaluated qualitatively with Analyse RayfleX v.2.352 software (Version 2.352, International Union of Crystallography, Chester, England). Some chemical mineral data were obtained by X-ray fluorescence spectrometry (RFA).

Geochronology: mechanical and chemical sample preparation for Rb-Sr analyses was performed at the Geological Survey of Austria in Vienna. Apophyllite crystals of >1 cm, several millimeter large prehnite aggregates, as well as defined parts of altered host rock were broken or cut off of hand specimens. They were then separately crushed in an agate hand mortar. After that, the mineral concentrates were refined under a binocular microscope, whereas the host rock samples were ground by hand in an agate mortar. The weights of the samples used for dissolution were about 200 mg for apophyllite and prehnite, and 100 mg for basalt powders. They were dissolved in a mixture of HF:HNO₃ = 4:1. Chemical sample preparation followed the procedure described by Sölva et al. [40].

Rb-Sr isotopic measurements were made at the Department of Lithospheric Research at the University of Vienna. Element concentrations were determined by isotope dilution using mixed Rb-Sr spikes. Isotopic ratios were measured with a ThermoFinnigan® Triton MC-TIMS (Thermo Fisher Scientific, Waltham, MA, USA). Sr was run from Re double filaments, whereas Rb was evaporated from a Ta single filament. Total procedural blanks were <1 ng for Rb and Sr. During the periods of measurement, the NBS987 standard yielded $^{86}\text{Sr}/^{87}\text{Sr} = 0.710248 \pm 4$ ($n = 17$) on the Triton TI. Ages were calculated with the software ISOPLOT/Ex [41], assuming an error of 1% on the $^{87}\text{Rb}/^{86}\text{Sr}$ ratio.

The separated size fraction of apophyllite was analyzed by the K-Ar method, following the procedure laid out by Balogh [42] in the K-Ar laboratory of the Institute for Nuclear Physics, Hungarian Academy of Sciences, Debrecen. Potassium content was measured on 50-mg sample aliquots, after dissolution by HF and HNO₃, with a Sherwood-400-type flame spectra-photometer with accuracy better than $\pm 1.5\%$. Separated mineral sample splits were then subjected to heating at 100 °C for 24 h under vacuum, to remove atmospheric Ar contamination that was adsorbed on the surface of the mineral particles during sample preparation. Argon was extracted from the minerals by fusing the samples via high-frequency induction heating at 1300 °C. The released gases were cleaned in two steps in a low-blank vacuum system by St-707 and Ti-getters. The isotopic composition of the spiked Ar was measured using a Nier-type mass spectrometer and corrected for the atmospheric $^{40}\text{Ar}/^{36}\text{Ar}$ ratios [43]. The accuracy and reproducibility of isotope ratio measurements were periodically controlled with the Rodina 2/65 internal standard. Decay constants recommended by Steiger and Jäger [44] were used for age calculation, with an overall error of $\pm 2\%$.

4. Results

4.1. Field Observations in the Quarries of Salsette Island

The Dahisar quarry complex was operated at an altitude between 30 to 130 m asl. During the field observation in the 1990s, the upper part (50 to 130 m asl.) was already overgrown by vegetation and no longer accessible for studying. The lower part consists mainly of hyaloclastites without pillows. In the other Salsette Island quarries, partly spilitized pillows, with hyaloclastite breccia in the interpillow spaces in between, were exposed. Intercalations of massive lava flows or intertrappeans were not observed.

4.1.1. Textures of Pillow Basalt and Hyaloclastite

Figure 3a shows a characteristic sequence of pillowed basalt and hyaloclastite in the Kurar quarry. The textures are not uniform, but rather show a diffuse layering. This is due to the density of pillowed basalt within the hyaloclastite matrix, which is also demonstrated by slight differences in color. Layers of densely packed pillows are greyish. The bottoms of the individual pillows have a convex shape and there is only a minor amount of hyaloclastite in the gaps in between. In contrast, layers rich in hyaloclastite are greenish, with more isolated pillows characterized by a round or oval shape and a concave bottom. The pillow size ranges between 20 cm and 100 cm.

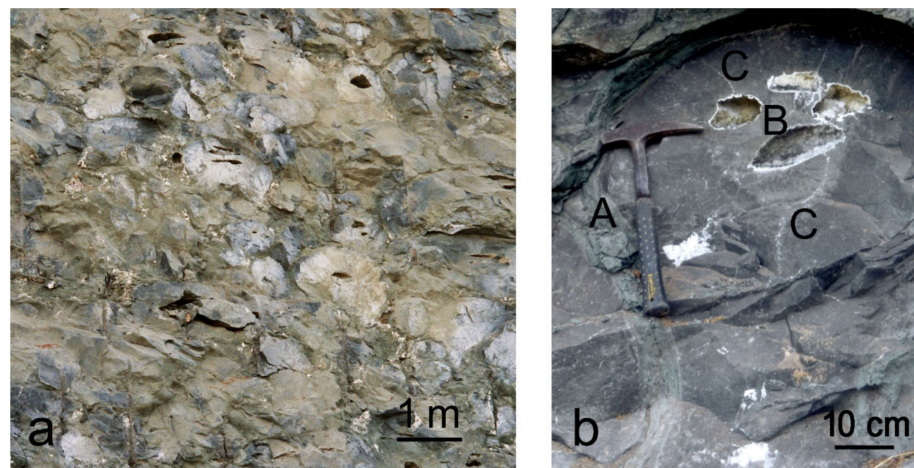


Figure 3. Textures of pillow basalt and hyaloclastite. (a) Photograph of a north–south section (north on the left side) of pillow basalt in the Kurar quarry, displaying a sequence of the irregular distribution of pillows and gaps between, filled by strongly altered hyaloclastite and pillow breccia. Cavities occur within pillows and void spaces appear in the breccia. (b) Section of a pillow with greenish selvage (A), several gas blister cavities (B), and radiating cracks (C).

Pillows show typical outer selvages of highly to completely altered basaltic glass formed during rapid cooling in water (Figure 3b). Cavities are frequently present in the central part of the pillows, which are also surrounded by thin selvages of highly altered basalt. The cavities are usually connected to the pillow outside by radiating cooling cracks, which are generally filled with laumontite.

The interior of the pillow matrix consists of grey-greenish, moderately to intensively spilitized basalt, with irregularly distributed spots of more freshly preserved, dark-grey basalt (Figure 4a). Angular fragments of brownish to greenish-gray altered basaltic glass and pillow basalt form the components of the hyaloclastite and pillow breccia (Figure 4b). They are predominately centimeter sized, but some fragments may reach up to several decimeters.

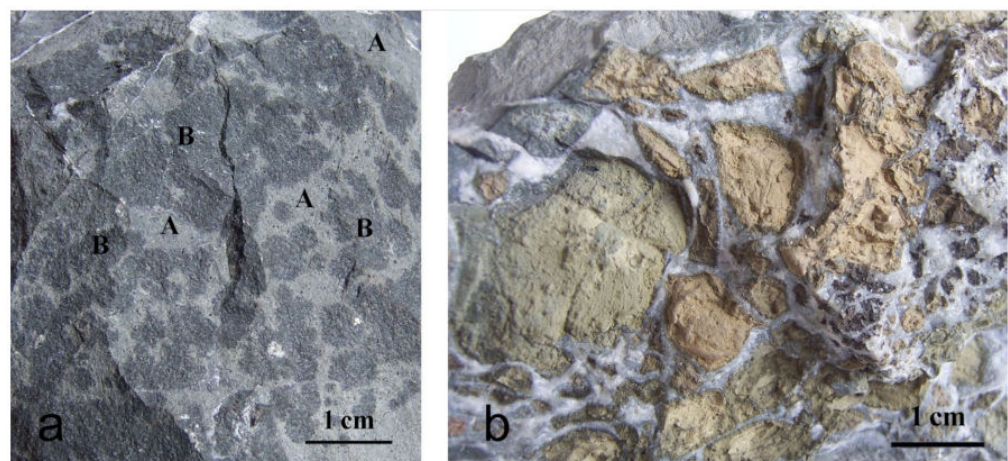


Figure 4. (a) Detail of a pillow core displaying a partly spilitized green-grey groundmass (A), with dark grey spots (B) of freshly preserved basalt. (b) Detail of hyaloclastite and pillow breccia with laumontite and other minor secondary minerals.

In thin sections of the freshly preserved dark grey basalt from the interior of the pillows, a fine grained matrix of plagioclase, pyroxene, opaque ore minerals, and glass in between is visible (Figure 5a). Up to a few-millimeter-sized plagioclase phenocrysts seldom occur therein. Sometimes they form aggregates of several crystals. Frequent bubbles are filled by concentrically zoned brownish, green-brownish, or yellowish palagonite. In the center,

greenish chlorite or colorless zeolites may be present. The fresh basalt is surrounded by altered basalt, with an irregularly shaped contact. In the altered basalt, the glass is replaced by palagonite, but magmatic plagioclase and pyroxene are at least partly preserved. The selvages towards the outside and along the cracks are highly, to completely, spilitized with dusty albite intergrown with zeolites and other minerals (Figure 5b).

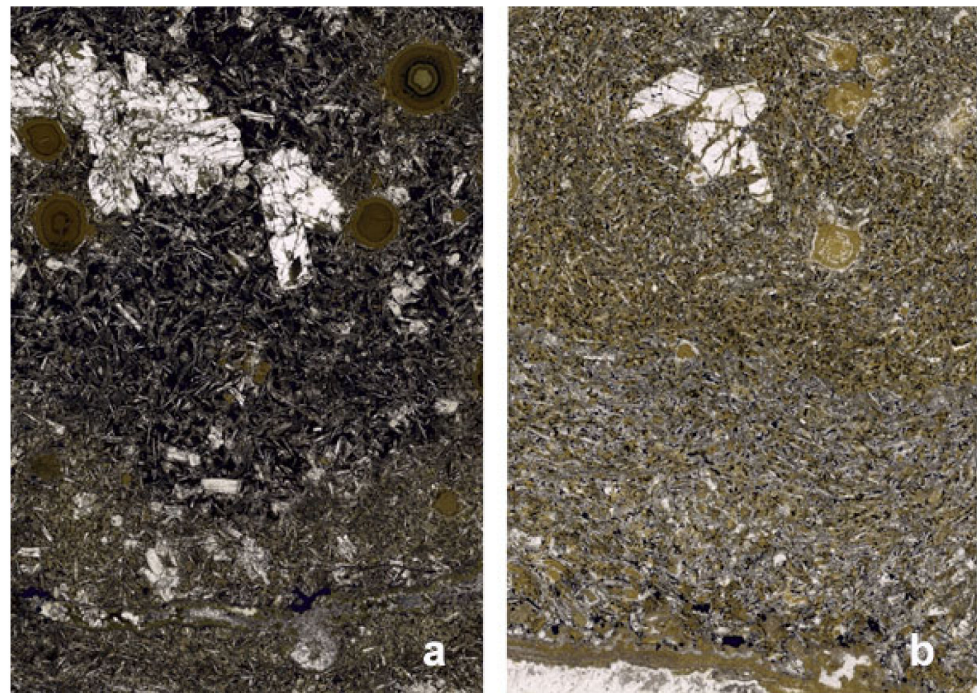


Figure 5. Thin section of pillow basalt. (a) Fresh basalt (dark upper part) with aggregate of plagioclase phenocrysts and altered basalt (lower part) (sample K1, field of view (fov) ca. 7 mm). (b) Altered basalt (upper part) and spilitized basalt (lower part). At the bottom, the margin of a cavity consisting of laumontite, calcite, and other minerals is visible (sample K2, fov ca. 3.5 mm).

4.1.2. Cavities in the Volcanic Rocks

Three types of cavities can be observed in the volcanic rocks. Original gas blisters occur within the pillows (Figure 3b). They are situated in the central to upper central part of the pillow and exhibit a shape with a concave section. The second type of cavities arises within pillow lobes formed when molten lava inside drains out to form pillow buds or pillow toes. These drained cavities are often characterized by multiple horizontal lava levels, called lava septa, between which more or less flat cavities have formed (Figure 6a,b) [45]. Even if their geometry differs from that of gas blisters, they still form closed cavities surrounded by massive basalt. No fundamentally different mineralization could be observed between the blister and the drained cavities. In less than 30% of the pillows, one or several cavities occur. Their size can range from a few centimeters up to about 30 cm in horizontal diameter. Generally, the cavities are only partly filled by secondary minerals (Figures 3b and 6a). A third type is represented by void spaces in the interpillow matrix. This results from gaps between the individual pillows that are not completely filled with breccia (Figure 6a,b). The void spaces in the interpillow matrix are characterized by an irregular shape and their size ranges from a few centimeters up to several decimeters (Figure 6a,b). Local quarry workers reported that in two exceptional cases the cavities in the Pathanwadi quarry were large enough for a man to stand inside. Small void spaces are commonly completely filled by laumontite and other minor secondary minerals, whereas larger ones are only partly filled.

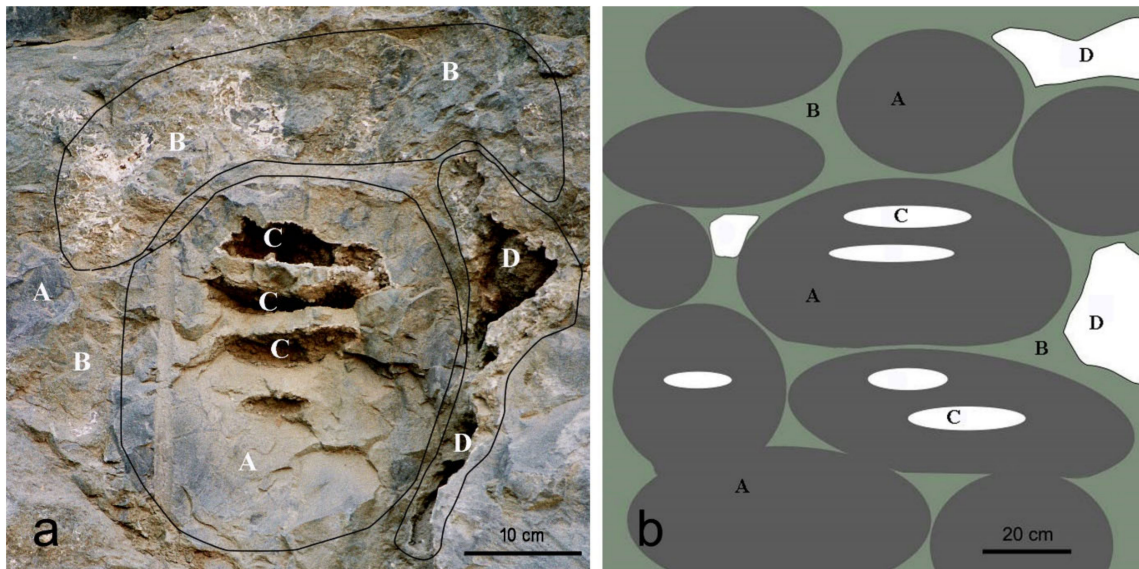


Figure 6. Cavities in a pillow and void spaces in the interpillow matrix. (a) Field photograph (section view) and (b) schematic sketch showing: (A) partly spilitized pillows, (B) interpillow matrix consisting of altered hyaloclastite breccia, (C) drained cavities within pillows, (D) void spaces.

Some of the secondary minerals occur all around on the cavity walls, without any preferred orientation (Figure 7a), whereas others tentatively appear only on the bottom or side. Occasionally, one or two horizontal crusts consisting of different minerals may be present in the lower part of the cavities (Figure 7a). However, in most cases, only remnants are attached to the cavity walls, whereas encrusted fragments appear on the cavity ground (Figure 7b).

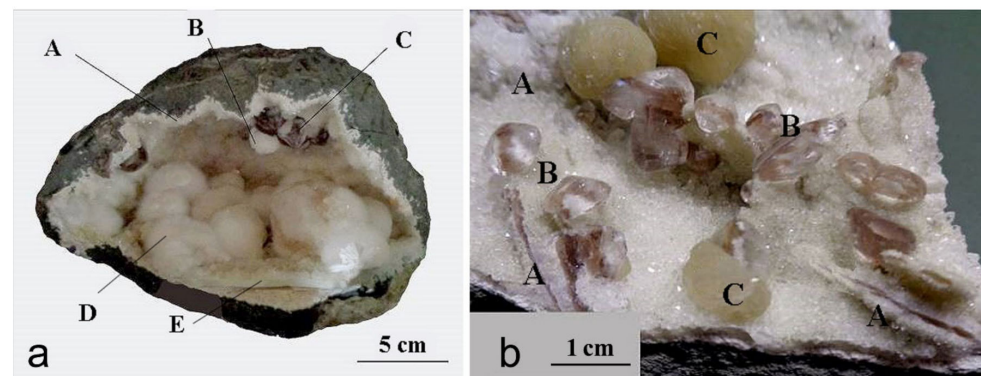


Figure 7. Photographs of hand specimens with secondary minerals and mineralized crusts. (a) Typical blister cavity from a pillow with slightly irregular, lenticular shape. The wall lining consists of tiny quartz crystals (A). Some secondary minerals such as gyrolite (B) and calcite (C) appear all around the cavity walls, whereas okenite (D) typically tends to occur at the bottom. In addition, at the bottom, remnants of a horizontal mineralized crust (E) are visible. (b) Detail from a bottom part of a pillow cavity: Fragments of brownish crust (A) are encrusted by quartz and overgrown by calcite (B) and gyrolite (C).

4.2. Secondary Minerals from the Cavities and Void Spaces

In this section, the secondary minerals from cavities and void spaces are described in chemical-alphabetical order. They include sulfides, oxides, hydroxides, carbonates, sulfates, and different types of silicates. Table 1 lists details about their frequency of occurrence within pillow cavities and void spaces. Examples of most of the minerals are shown in Figure 8 and several chemical analyses are presented in Table 2.

Table 1. Frequency of the secondary minerals from the cavities and void spaces from Salsette Island. X—very rare, XX—rare, XXX—frequent, XXXX—common.

Mineral	In Pillow	In Void Space	Mineral	In Pillow	In Void Space
Sulfides			Sorosilicates		
Chalcopyrite		x	Prehnite	XXX	XXXX
Sphalerite		X	Pumpellyite-(Fe ²⁺)	x	
Galena		X	Inosilicates		
Pyrite	XX	XXX	Babingtonite		XX
Oxides, Hydroxides			Okenite	XXXX	XXX
Hematite	X	XXX	Phyllosilicates		
Quartz	XXXX	XXXX	Chlorite	XXX	XXXX
Ferberite		x	Apophyllite-(K)	XXX	XXXX
Carbonates			Gyrolite	XXXX	XXXX
Calcite	XXXX	XXXX	Zeolites		
Aragonite			Chabazite-Ca	XX	
Sulfates			Epistilbite	XX	
Gypsum		X	Heulandite-Ca	XX	
Neosilicates			Laumontite	XXXX	XXXX
Andradite		X	Natrolite	XX	
Sorosilicates			Scolecite	XX	
Ilvaite	X		Stilbite-Ca	XX	
Julgoldite-(Fe ²⁺)		X	Yugawaralite	X	XX



Figure 8. Cont.



Figure 8. Photographs of secondary minerals from Salsette Island. (a) Chalcopyrite; (b) Sphalerite and galena as vein filling; (c) Pyrite as dodecahedron with gyrolite; (d) Hematite; (e1) Quartz, (e2) quartz precipitated on a brownish crust; (f1) Brown calcite I overgrown by quartz, colorless calcite II and yellow chabazite; (f2) Calcite II with flat brown central zone, gyrolite, okenite, and laumontite; (f3) Aragonite; (g) Gypsum with apophyllite-(K); (h) Andradite (yellow) with prehnite; (i) Ilvaite; (j) Julgoldite-(Fe²⁺); (k1) Yellow prehnite; (k2) Casts of green prehnite after laumontite. (l) Pumpellyite-(Fe²⁺) on ilvaite; (m) Babingtonite with quartz; (n) Okenite; (o) Apophyllite-(K) with okenite and quartz; (p1) Gyrolite; (p2) Schematic section through a gyrolite sphere, increasing Fe, Mn content; (q) Chabazite-Ca; (r) Epistilbite; (s) Heulandite-Ca with pink chabazite-Ca; (t) Laumontite with gyrolite; (u1) Natrolite; (u2) Green scolecite with red stilbite-Ca and altered apophyllite-K; (v) Chlorite with quartz and prehnite; (w) Red stilbite-Ca with calcite; (x) Yugawaralite.

4.2.1. Sulfides

Chalcopyrite CuFeS₂ (Figure 8a) appears as idiomorphic crystals with the form {211} and can be up to 5 mm in size. The mineral was only detected in void spaces of highly altered hyaloclastite breccia on top of the quartz lining in the Dahisar quarry.

Sphalerite ZnS and Galena PbS (Figure 8b) occur as vein fillings in the Dahisar quarry. Sphalerite with small spots of galena formed a 1–3 mm thick layer of ~25 cm² total on one side of a hand sized specimen.

Pyrite FeS₂ (Figure 8c) appears as 0.2–1.0 mm sized xenomorphic aggregates in highly altered basalt but also as idiomorphic well-developed crystals up to 10 mm in size within the cavities of the pillows. The predominant form is the {210}. The isomorphous crystals are precipitated on quartz and associated with calcite, prehnite, gyrolite, and hematite. Pyrite crystals from the Dahisar quarry exclusively developed the form {100}.

4.2.2. Oxides, and Hydroxides

Hematite Fe_2O_3 (Figure 8d) occurs in the void spaces of the hyaloclastite breccia as bladed crystals, forming rosette-like hemispheres. In the Kurar quarry, it is associated with calcite, prehnite, gyrolite, quartz, and pyrite and reaches 10 mm in diameter. In the Dahisar quarry, large hemispheres up to 20 mm in size were found.

Quartz SiO_2 (Figure 8e1,e2) occurs very commonly, but in different modes. Most common are the up-to-5-mm-long clear crystals forming the wall lining in the cavities. They exhibit a habit of prism {100} and both main rhombohedra {011}, {101}. Such a quartz wall lining is underlain by a very thin layer of laumontite and occasionally by brown calcite I crystals. All the other secondary minerals appear on top of the quartz wall lining. In a fractured, light grey colored and strongly altered hyaloclastite breccia of the Kurar quarry, the void spaces contained quartz crystals up to 5 cm in length. They were associated with natrolite/scolecite and apophyllite-(K). In the same zone, unusually formed crusts are found at the bottom of some void spaces. They form clusters connected by later mineral overgrowths. On one side of the plates, quartz crystals with a short prism and a diameter of 3 cm (Figure 8e2) developed, whereas the other side is overgrown by short 5 to 10 mm long quartz crystals, prehnite, and apophyllite-(K). Remarkably, cryptocrystalline quartz varieties (e.g., chalcedony) are not detected on Salsette Island.

Ferberite $\text{Fe}^{+2}\text{WO}_4$ crystals were only observed once in the void spaces of the hyaloclastite breccia, between the pillows in the Kurar quarry. The black platy crystals are characterized by the forms {100}, {102}, {111}, and {110}, forming sprays up to 10 mm in size. Ferberite is precipitated after prehnite and is associated with quartz.

4.2.3. Carbonates

Calcite CaCO_3 (Figure 8f1,f2) counts in the Kurar quarry as the most frequently occurring secondary mineral, and it often appears in two generations. In the pillow cavities, the first generation is deposited directly on chlorite, before the first laumontite precipitation. This early calcite I reaches 5 cm in size and develops a flat rhombohedral habit with a black to brownish color. It is generally overgrown by laumontite and wall lining quartz. The second generation (calcite II) is formed after quartz. It frequently developed on crusts in pillow cavities (Figure 7b) and reaches up to 3 cm in size. Two growth phases can be recognized for calcite II. During the first phase, dark brown crystals with a flat rhombohedral form were precipitated. In the second phase they are overgrown in a phantom-like manner by colorless calcite with a dipyramidal habit, composed of several different rhombohedral and scalenohedral forms (Figure 8f2). The brownish color of calcite I is due to dispersed Al-Mg-Fe phyllosilicates (pers. com. Pöhlmann, 1996).

Calcite is also the dominant mineral in the hyaloclastite breccia from the Dahisar quarry. Crystals of the first generation (calcite I) developed two different forms. The first, predominant, form is scalenohedral, with crystals up to 10 cm in length, occasionally overgrown by macrocrystalline quartz. Second, distorted rhombohedral crystals with tabular to lamellar habit are found, which are generally overgrown by green prehnite. The second generation (calcite II) is characterized by combinations of steep scalenohedra and rhombohedra. While the calcite from the pillow cavities does not show any fluorescence under short or long wave UV light, the second calcite generation (calcite II) from the Dahisar quarry shows an intensive red fluorescence under UV light (254 nm), probably due to traces of Mn. Additionally, yellow-colored, up-to-7-cm-long calcite crystals with significant prism faces were found in the Pathanwadi quarry. Argonite CaCO_3 (Figure 8f3) was discovered only once, as up-to-7-cm-long crystals, situated on laumontite.

4.2.4. Sulfates

Gypsum CaSO_4 (Figure 8g) belongs to the latest mineral phases and only occurs rather rarely. Clear idiomorphic crystals with a characteristic monoclinic habit reach up to 5 cm in size. They were found in the void spaces of the hyaloclastite breccia between the pillows in the Kurar quarry, deposited on prehnite.

4.2.5. Silicates

Nesosilicates

Andradite $\text{Ca}_3\text{Fe}^{3+}_2(\text{SiO}_4)_3$ (Figure 8h) is one of the very rare minerals found in the void spaces of the hyaloclastite breccia in the Kurar quarry. Wise and Moller [39] described hydro-andradite, which is an OH-containing variety of andradite. It forms yellowish transparent crystals up to 1 mm in size, and is associated with julgoldite, hematite, and quartz.

Sorosilicates

Ilvaite $\text{CaFe}^{3+}\text{Fe}^{2+}_2\text{O}(\text{Si}_2\text{O}_7)(\text{OH})$ (Figure 8i) belongs to the group of Ca-Fe-silicates. Rarely, it has been detected in pillow cavities as prismatic crystals, occasionally reaching more than 10 mm in length. The shape of the dipyrnidal crystals is characterized by the forms {112}, {110}, and {010}. Dull black spheres of pumpellyite are commonly grown on the high gloss prism faces. Ilvaite is associated with quartz, calcite, laumontite, gyrolite, and okenite.

Prehnite $\text{Ca}_2\text{Al}(\text{Si}_3\text{Al})\text{O}_{10}(\text{OH})_2$ (Figure 8k1,k2) appears frequently as rhombic crystals, typically forming spherical aggregates with a diameter up to ca. 8 mm. Single crystals always exhibit a tabular curved habit. Spherical aggregates are occasionally present in the cavities of the pillows, sitting directly on the quartz wall lining or on laumontite. In the void spaces of the hyaloclastite breccia, prehnite is common. The perimorphs of prehnite after laumontite from the void spaces are remarkable. When laumontite was dissolved, the casts represented perimorphs of prehnite after laumontite (Figure 8k2). Pale green prehnite contains up to 2.5 wt% Fe_2O_3 , whereas the rarer yellowish variety is characterized by a Fe_2O_3 content of only about 0.5 wt%. Furthermore, the Fe_2O_3 content in the prehnite of the pillow cavities is significantly lower than that in the void spaces. The pale green prehnite perimorphs after laumontite contain up to 4 wt% Fe_2O_3 , partly replacing Al_2O_3 .

Pumpellyite-(Fe^{2+}) $\text{Ca}_2\text{Fe}^{2+}\text{Al}_2(\text{Si}_2\text{O}_7)(\text{SiO}_4)(\text{OH},\text{O})_2\cdot\text{H}_2\text{O}$ (Figure 8l) belongs to the seldom discovered Ca-Fe-silicates. The greenish-black mineral forms spherical aggregates up to 5 mm in size, resting predominantly on the prism faces of ilvaite. Pumpellyite has not been detected together with julgoldite or babingtonite. Julgoldite-(Fe^{2+}) $\text{Ca}_2\text{Fe}^{2+}\text{Fe}^{3+}_2(\text{Si}_2\text{O}_7)(\text{SiO}_4)(\text{OH})_2\cdot\text{H}_2\text{O}$ (Figure 8j) is the iron-rich endmember of the pumpellyite group. It is present in the void spaces of the hyaloclastite breccia, as thin tabular black crystals up to 20 mm in length. It is associated with chlorite, prehnite, andradite, hematite, and quartz.

Inosilicates

Babingtonite $\text{Ca}_2\text{Fe}^{2+}\text{Fe}^{3+}\text{Si}_5\text{O}_{14}(\text{OH})$ (Figure 8m) is found in the hyaloclastite breccia of all of the quarries except Dahisar. The black and highly lustrous crystals are up to 10 mm in size and clearly display the triclinic symmetry, with the forms {110}, {001}, {100}, {101}, {210}, and {111}. Most commonly, it is in association with quartz and prehnite.

Okenite $\text{Ca}_{10}\text{Si}_{18}\text{O}_{46}\cdot 18\text{H}_2\text{O}$ (Figure 8n) counts as one of the commonly occurring minerals in the cavities of the pillows. It forms radiating aggregates of white, up to 20 mm long fibrous crystals, associated with quartz, laumontite, prehnite, calcite, and gyrolite. Okenite was also found in the void spaces of the hyaloclastite breccia as spherical aggregates up to 10 mm in diameter and was deposited on prehnite.

Phyllosilicates

Chlorite group–Clinochlore $\text{Mg}_5\text{Al}(\text{AlSi}_3\text{O}_{10})(\text{OH})_8$ is the first precipitated mineral, rarely forming spherically aggregates of idiomorphic crystals up to 2 mm in diameter (Figure 8v). It is commonly overgrown by laumontite, quartz, or prehnite.

Apophyllite may occur as fluorapophyllite-(K) $\text{KCa}_4(\text{Si}_8\text{O}_{20})(\text{F},\text{OH})\cdot 8\text{H}_2\text{O}$ and hydroxyapophyllite-(K) $\text{KCa}_4\text{Si}_8\text{O}_{20}(\text{OH},\text{F})\cdot 8\text{H}_2\text{O}$ (Figure 8o). According to Ottens [19], the content of F in apophyllite from Salsette Island is variable, with an average value of 0.45 wt%. Due to the low fluorine content, it can be regarded as an intermediate member

of the apophyllite-(K) subgroup and is therefore referred to as apophyllite-(K) in the following. It exhibits short prismatic to blocky crystals, with the forms {110}, {001}, and minor {101}. The commonly colorless crystals reach 20 mm in size. Apophyllite-(K) occurs predominantly on prehnite within the void spaces of the hyaloclastite breccia and is occasionally found together with calcite, laumontite, gyrolite, and okenite within pillow cavities. The color of the very rarely occurring green varieties present in the void spaces is due to a V content of approximately 500 to 1500 ppm [46].

Gyrolite $\text{NaCa}_{16}(\text{Si}_{23}\text{Al})\text{O}_{60}(\text{OH})_8 \cdot 14\text{H}_2\text{O}$ (Figure 8p1,p2) is one of the most frequent minerals in the pillow cavities. The very thin lamellar hexagonal crystals form spherical aggregates with a diameter of up to 5 cm and aggregate clusters of up to 30 cm. Gyrolite is deposited directly on laumontite or quartz wall lining and predates precipitation of okenite. It is usually white in color, but green, and brown to black varieties are also observed. In some cases, the colored spheres show a white center and colored overgrowths. The color is due to Fe and Mn contents [39], reaching up to 3500 ppm and 2800 ppm, respectively.

Tectosilicates–Zeolites

Chabazite-Ca $\text{Ca}_2[\text{Al}_4\text{Si}_8\text{O}_{24}] \cdot 13\text{H}_2\text{O}$ (Figure 8q) is present in the pillow cavities and forms crystals up to 2 cm in size. The color is commonly white but can also tend towards salmon-like pink or yellow. The habit is formed by rhombohedra. The mineral is associated with quartz, calcite, only occasionally with scolecite, and remarkably frequently with epistilbite. Chabazite was also detected as 0.1 mm sized crystals together with okenite on apophyllite, probably formed as a late second generation in the void spaces.

Epistilbite $\text{Ca}_3[\text{Si}_{18}\text{Al}_6\text{O}_{48}] \cdot 16\text{H}_2\text{O}$ (Figure 8r) belongs to the zeolites rarely occurring in the cavities of the pillows. The white tabular crystals are up to 10 mm in size and are dominated by the forms {110}, {112}, and {101}. They are generally twinned on the twinning plane (100).

Heulandite-Ca $(\text{Ca},\text{Na},\text{K})_5(\text{Si}_{27}\text{Al}_9)\text{O}_{72} \cdot 26\text{H}_2\text{O}$ (Figure 8s) rarely occurs in the cavities of the pillows. It appears as white crystals up to 3 cm in size, sitting directly on the quartz wall lining. The habit is dominated by the form {010}, exhibiting slightly curved faces. The mineral is associated with calcite, chabazite, and scolecite. Additional EDX-analyses indicate Na and Sr contents of 1.57 wt.% and 0.4 wt.%, respectively. Such varieties should be classified as sodium-strontium bearing heulandite-Ca.

Laumontite $\text{CaAl}_2\text{Si}_4\text{O}_{12} \cdot 4\text{H}_2\text{O}$ (Figure 8t) is a widespread zeolite, forming masses and crystals up to 15 cm in length within the void spaces of the interpillow breccia, and crystals of up to 5 cm in the pillow cavities. The large crystals display a monoclinic habit with the forms {100} and {110}. The first laumontite precipitation (laumontite I) in the pillow cavities is present as a thin (ca. 1 mm) layer covering the altered host rock or chlorite, and is in turn overgrown by the quartz wall lining. The second generation (laumontite II) is represented by elongated idiomorphic crystals appearing on quartz. It is commonly associated with gyrolite and okenite. In the void spaces of the hyaloclastite breccia, laumontite II is often completely overgrown by prehnite. After the opening of a pillow cavity, freshly extracted laumontite crystals are transparent and display a pink color and sharp crystal edges. In dry air, they change their original structure by the loss of 1/8 of the chemically bounded H_2O . The quick dehydration process causes a metamorphosis into the variety leonhardite, a very soft material, which decomposes to a dusty powder with the weakest mechanical loads. Additionally, laumontite III is present as thin coatings, also present on prehnite. In general, laumontite is very pure, with a negligible Fe content according to RFA analyses.

Natrolite $\text{Na}_2(\text{Si}_3\text{Al}_2)\text{O}_{10} \cdot 2\text{H}_2\text{O}$, Mesolite $\text{Na}_2\text{Ca}_2(\text{Si}_9\text{Al}_6)\text{O}_{30} \cdot 8\text{H}_2\text{O}$, and Scolecite $\text{Ca}(\text{Si}_3\text{Al}_2)\text{O}_{10} \cdot 3\text{H}_2\text{O}$ (Figure 8u1,u2) are three members of the natrolite group. They are described together, because at Salsette Island they occasionally occur as epitaxial intergrowths. First, scolecite was precipitated, followed occasionally by a transitional zone of mesolite, and finally by natrolite. This was revealed by chemical element mapping of a 1 mm thick (cross section) crystal by SEM-EDX, which showed a core of scolecite and an approximately 40- μm -thick Na rich rim. The needle-like crystals are usually colorless, reach 10 cm in

length, and are grouped in radiating aggregates. All crystals display a pseudo-tetragonal habit by the forms {110} and {111}. The crystals are situated directly on the quartz wall lining and are associated with laumontite, prehnite, and calcite, and seldomly with stilbite. Occasionally, the crystals consist mainly of scolecite and contain green inclusions of a clay mineral.

Stilbite-Ca $\text{NaCa}_4(\text{Si}_{27}\text{Al}_9)\text{O}_{72}\cdot 28\text{H}_2\text{O}$ (Figure 8w) is rarely observed as white to cream or reddish colored crystals reaching up to 4 cm in size. It is associated with calcite, quartz, and scolecite.

Yugawaralite $\text{Ca}(\text{Si}_6\text{Al}_2)\text{O}_{16}\cdot 4\text{H}_2\text{O}$ (Figure 8x), belonging to the worldwide rare zeolites, was discovered as unusually big crystals of up to 8 cm in size. They are tabular to lath-like, flattened parallel to the most prominent form {010}, and elongated along the a-axis. Some larger crystals occur in elongated tabular aggregates of several individuals oriented parallel to {010}. The central crystals of the aggregates tend to be the thickest and longest with progressively thinner and shorter crystals outward along the b-axes. Yugawaralite occurs in the cavities of the pillows and in the void spaces of the hyaloclastite breccia. It was precipitated after the first laumontite generation and the quartz wall lining. Prehnite and babingtonite also grew earlier, whereas gyrolite and okenite formed later on.

Table 2. Chemical composition (wt.%) of the most common secondary minerals from Salsette Island.

	1	2	3	4	5	6	7
	Laumontite	Stilbite-Ca	Heulandite-Ca	Chabazite-Ca	Natrolite	Scolecite	Yugawaralite
SiO ₂	51.86	57.26	58.27	52.73	47.39	45.70	60.38
Al ₂ O ₃	21.28	15.29	16.19	16.35	26.84	24.90	16.58
Fe ₂ O ₃	<0.01	<0.01	<0.01	0.54	0.46	<0.01	<0.01
CaO	13.09	8.49	7.10	8.02	0.15	15.11	10.41
MgO	0.04	0.02	0.02	n.d.	n.d.	0.05	0.03
BaO	n.d.	n.d.	0.09	n.d.	n.d.	n.d.	n.d.
SrO	n.d.	n.d.	0.40	n.d.	n.d.	n.d.	n.d.
Na ₂ O	<0.01	0.52	1.59	0.69	14.48	n.d.	<0.01
K ₂ O	0.02	n.d.	0.33	1.02	0.02	n.d.	n.d.
l.o.ign.	13.57	18.29	15.85	20.00	10.86	14.00	12.23
Total	99.88	99.88	99.88	99.35	100.20	99.77	99.92
	8	9	10	11	12	13	14
	Epistilbite	Apophyllite-K	Okenite	Gyrolite	Prehnite	Calcite I	Chlorite
SiO ₂	58.20	52.70	53.47	53.88	42.53	0.20	29.05
Al ₂ O ₃	16.68	0.17	0.04	2.21	21.01	<0.01	10.54
FeO	n.d.	n.d.	n.d.	n.d.	n.d.	n.d.	27.63
Fe ₂ O ₃	<0.01	n.d.	<0.01	0.45	3.93	1.42	n.d.
CaO	0.99	25.62	28.58	30.02	27.88	55.50	0.23
MgO	0.02	n.d.	n.d.	n.d.	0.06	0.20	15.61
MnO	0.01	n.d.	n.d.	n.d.	n.d.	n.d.	0.47
Na ₂ O	0.95	n.d.	n.d.	0.26	n.d.	n.d.	n.d.
K ₂ O	0.01	4.22	n.d.	0.02	n.d.	n.d.	n.d.
o ⁻²	n.d.	-0.19	n.d.	n.d.	n.d.	n.d.	n.d.
l.o.ign.	15.01	16.98	16.81	12.41	4.44	42.56	n.d.
Total	99.88	99.95	99.91	99.26	99.88	99.88	99.88

Comments: (1) For analyses, a freshly preserved laumontite, protected in an airtight box after extraction in the quarry, and was used. (2) White stilbite-Ca is characterized by low Fe₂O₃ contents, the red variety contains up to 0.08 wt%. (5) The sample is an epitaxial overgrowth from natrolite on scolecite. Pure natrolite was not detected. (12) The characteristically green color of prehnite from a void space is due to a Fe₂O₃ content. N.d. – not determined.

4.3. Summarized Mineralization Sequence

Based on the observations in the quarries and hand specimens, a general mineralization sequence for the secondary minerals in void spaces of the hyaloclastite breccia and the pillow cavities can be summarized as follows:

Void spaces: chlorite → laumontite I (masses) → calcite I (often partly dissolved) → laumontite II (big crystals) → quartz → babingtonite → yugawaralite → prehnite (overgrown on laumontite II) → julgoldite → calcite II → laumontite III → gyrolite → okenite → apophyllite-(K).

Zeolites such as heulandite-Ca, stilbite-CA, epistilbite, natrolite/scolecite, and chabazite-Ca are absent in the void spaces. Calcite II and quartz occur only rarely. Prehnite commonly forms perimorphs after laumontite II. The number of secondary mineral species and their volume vary significantly between individual void spaces.

Pillow blister and drained cavities: chlorite → calcite I (often partly dissolved) → laumontite I (thin crust) → quartz → laumontite II (big crystals), prehnite (no perimorphs after laumontite) → calcite II → ilvaite → pumpellyite → gyrolite → laumontite III → okenite → natrolite/scolecite → heulandite-Ca → stilbite-Ca → epistilbite → apophyllite-(K) → chabazite-Ca.

In the pillow blister and drained cavities, prehnite occurs as single spherical aggregates on quartz. The zeolites heulandite-Ca, stilbite-Ca, epistilbite, scolecite/natrolite, and chabazite-Ca occur only rarely. Generally, the number of mineral species present does not vary significantly between the individual pillow cavities. The position of the minerals shows common characteristics, whereby the early precipitated minerals (calcite I, laumontite I, quartz, and calcite II) occur all around the cavity walls, without any preference, and the later formed minerals (like okenite) appear only tentatively on the bottom or sides.

4.4. Geochronology

Geochronological investigations on apophyllite-(K) were performed, to obtain some time constraints on the formation of the secondary mineralization. Apophyllite-(K) contains about 3–5 wt.% K₂O and high Rb/Sr ratios suitable for the K-Ar and Rb-Sr methods, respectively. For the latter method, additional data points with low Rb/Sr ratios are necessary for age calculations. Two samples, one from a void space within the hyaloclastite breccia (BOM-3) and the other from a pillow cavity (K4a), both from the Kurar quarry, were investigated. Analytical results are presented in Figure 9 and Tables 3 and 4.

Table 3. K isotopic data apophyllite (App) from the Deccan volcanic province (India) near Mumbai. In comparison the corresponding Rb-Sr ages are given. For an explanation see text.

Sample	Material	Laboratory	K	⁴⁰ Ar rad	⁴⁰ Ar rad	K-Ar Age	Rb-Sr Age
		number	(%)	(ccSTP/g)	(%)	(Ma) (±1σ)	(Ma) (±2σ)
BOM-3	App	8700	3.081	3,3066E-06	32.0	27.4 ± 1.5	29.19 ± 0.29

A piece of greenish-grey slightly altered basalt from about 2 cm below the quartz wall lining and another piece of bright greenish-grey spilitized basalt selvage, forming a 3 mm wide layer in contact with the quartz lining, were separated from the sample (K4a). Additionally, 3 mm large spherical prehnite aggregates overgrown by a thin crust of laumontite, and a 16 mm long and 10 mm wide apophyllite-(K) crystal situated on top of the quartz wall lining, were extracted. From the second sample (BOM-3), massive pale green prehnite and a pseudocubic apophyllite-K crystal with about 1-cm edge length sitting on top of it were prepared.

The slightly altered basalt (WR) and the spilitized selvage (Sel) at the cavity margin show strongly different Rb and Sr contents, with higher values in the less altered basalt. With respect to the geochemical data in Patel et al. [6], from nearby Elephanta Island, the Rb contents are in the range of fresh tholeiitic basalt (0.1–20 ppm), whereas the Sr content (ca. 220 ppm) is considerably lower. The measured ⁸⁷Sr/⁸⁶Sr ratios are in the

range of published data for fresh tholeiitic basalt [6] and spilitized basalts of Salsette Island [47] (0.70391–0.70784), and the initial $^{87}\text{Sr}/^{86}\text{Sr}$ calculated for 65 Ma (K4a WR = 0.70568; K4a Sel = 0.70566) are also comparable (0.7039–0.7045 but up to 0.7079). The investigated prehnite yielded low Rb and Sr contents of about 0.1 to 2.6 ppm and 5.5 to 7.8 ppm, respectively, causing low $^{87}\text{Rb}/^{86}\text{Sr}$ ratios (0.03 and 1.38) and $^{87}\text{Sr}/^{86}\text{Sr}$ ratios in the range of those of the basaltic rocks. Apophyllite-K concentrates are characterized by Rb and Sr contents of about 130 and 1 ppm, respectively. These values fit those reported by Ottens et al. [14]. Accordingly, high $^{87}\text{Rb}/^{86}\text{Sr}$ ratios in the range of 270–340 were detected. From all data points of sample K4a, an age of 40.95 ± 0.41 Ma was calculated, whereas sample BOM-3 yielded 29.19 ± 0.29 Ma.

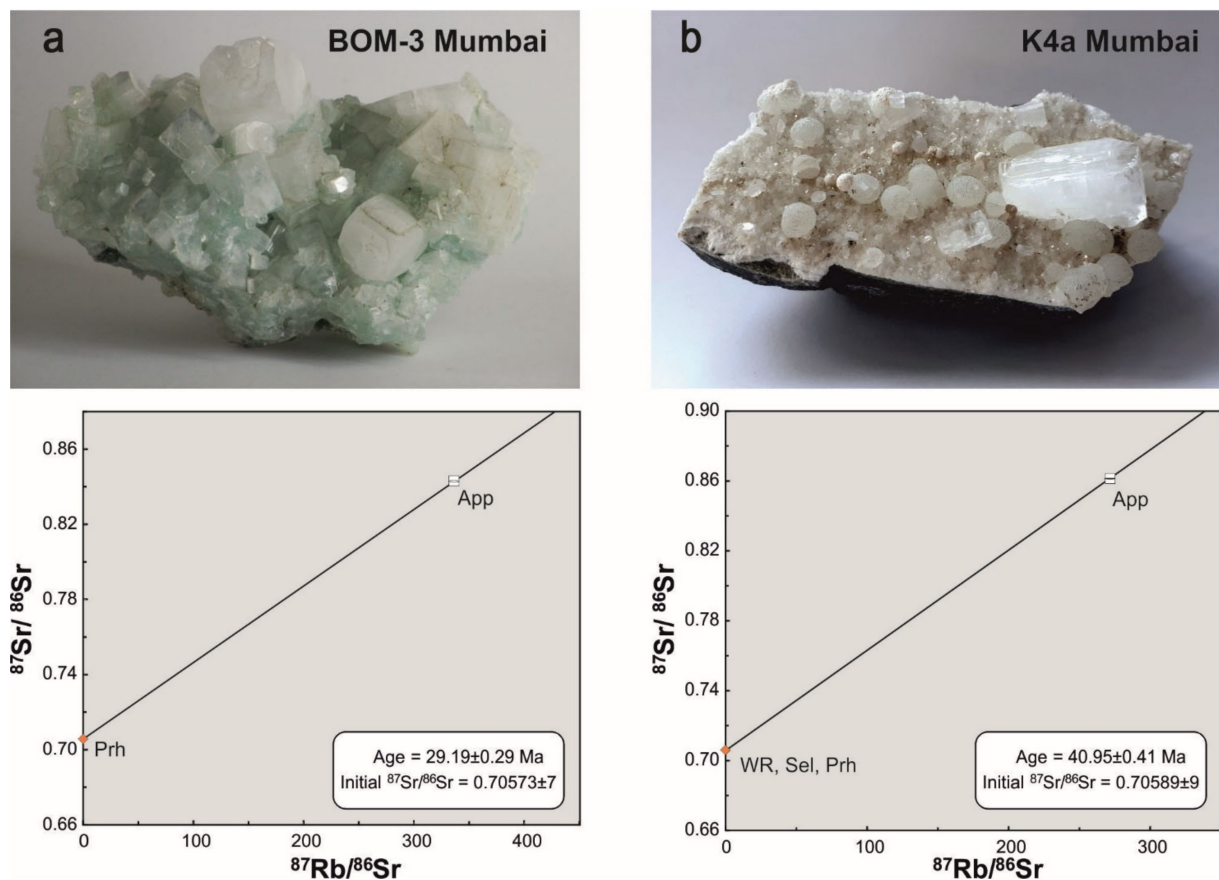


Figure 9. Rb-Sr age data from Salsette Island. (a) Sample BOM-3 derived from a void space within hyaloclastite breccia of the Kurar quarry. Blocky apophyllite is grown on greenish prehnite (wide of specimen 10 cm). The age was calculated from prehnite (Prh) and apophyllite-K (App). (b) Sample K4a was collected from a pillow cavity from the Kurar quarry. In contact with the cavity, the basalt shows a 3-mm-thick spilitized selvage. The secondary mineralization includes a thin layer mostly consisting of laumontite and calcite, overgrown by quartz. On top, spherical prehnite aggregates and up to 2 cm large apophyllite-K crystals are situated (wide of specimen 8 cm). For age calculation, basaltic whole rock (WR), selvage (Sel), prehnite (Prh), and apophyllite-K (App) were used. Both calculations are based on an error of $\pm 1\%$ on the $^{87}\text{Rb}/^{86}\text{Sr}$ ratio.

The apophyllite-(K) concentrate of sample BOM-3 contained 3.08 wt% K (corresponding to 3.71 wt% K_2O). The amount of radiogenic ^{40}Ar was 32.0%, and the determined K-Ar age was 27.4 ± 1.2 Ma. An interpretation of the age data is given in the discussion.

Table 4. Rb-Sr isotopic data on whole rock (WR), selvage (Sel), prehnite (Prh), and apophyllite (App) from the Deccan volcanic province (India) near Mumbai. Rb-Sr ages were calculated assuming an error of $\pm 1\%$ on the $^{87}\text{Rb}/^{86}\text{Sr}$ ratio.

Sample	Material	Rb (ppm)	Sr (ppm)	$^{87}\text{Rb}/^{86}\text{Sr}$	$^{87}\text{Sr}/^{86}\text{Sr}$	$\pm 2\sigma_m$	Age (Ma) ($\pm 2\sigma$)
K4a	WR	21.00	96.08	0.6324	0.70626	0.000006	
K4a	Sel	3.469	48.70	0.2061	0.70585	0.000004	
K4a	Phr	2.649	5.563	1.3782	0.70684	0.000026	
K4a	App	142.7	1.541	272.00	0.86148	0.000093	40.95 \pm 0.41
3-BOM	Phr	0.082	7.771	0.0305	0.705745	0.000004	
3-BOM	App	126.6	1.104	336.32	0.842906	0.000011	29.19 \pm 0.29

5. Discussion

Field observations and the study of hand specimens revealed a number of secondary minerals present in the void spaces of the hyaloclastite breccia and pillow cavities from Salsette Island. Their overgrowing textures in combination with the analytical data presented here, and in comparison to data in prior literature, allow a discussion of several aspects of their genesis.

More or less precise formation temperatures of the individual minerals can be found in the existing literature, and additional information comes from the fluid inclusions measured on calcite. With this data it is possible to estimate whether the precipitation sequence reflects simple cooling after eruption of the volcanic host rocks, or a more complex thermal history with episodes of reheating. Aspects of the temporal evolution are given by the timing of the magmatic event and the geochronological age data measured on apophyllite. The determined formation history can be related to that of the tholeiitic host rock and the regional geological evolution. Finally, the results from Salsette Island can be compared to other occurrences of secondary minerals in tholeiitic volcanic provinces.

5.1. Minerals and Aspects of Formation Temperatures and Physical Conditions

Most of the secondary minerals in the void spaces of the hyaloclastite breccia and the pillow cavities from Salsette Island are typical for zeolite facies and prehnite–pumpellyite facies in basaltic rocks. In general, diverse zeolites (e.g., laumontite, wairakite, heulandite), albite, quartz, and calcite are typical for the zeolite facies, whereas prehnite, pumpellyite, quartz, chlorite, albite along with titanite, and epidote appear in the prehnite–pumpellyite facies [48]. Their formation is associated with the breakdown of the basaltic mineral assemblage (calcic plagioclase, olivine, pyroxene, and glass) in contact with fluid during prograde burial metamorphism [49] and/or by hydrothermal processes, often induced by ongoing magmatic activity [50]. Field observations and the study of hand specimens revealed a number of secondary minerals present in the void spaces of the hyaloclastite breccia and pillow cavities from Salsette Island. Their overgrowing textures, in combination with the analytical data presented here and in comparison with data in prior literature, allow a discussion of several aspects of their genesis.

Even if the P-T fields for the various low-grade metamorphic facies are overlapping, the following ranges can be given [48]: The zeolite facies extend from about 50 °C to ca. 200 °C, but some zeolites (e.g., wairakite) appear up to >350 °C, at pressures below 4 kbar. The prehnite–pumpellyite facies, *sensu stricto*, cover a restricted field at 180–270 °C and up to 4 kbar. However, they are overlapped by prehnite-actinolite and pumpellyite-actinolite facies, which define a field at 220–350 °C and up to 9 kbar, whereby prehnite is stable at lower pressures. The lower limit of the greenschist facies can be estimated to be 250–350 °C. These values, determined by thermodynamic calculations by Frey et al. [48], fit the variable temperatures proposed from field observations. For example, Coombs et al. [49] described the transition from the zeolite facies to the prehnite–pumpellyite facies at ca. 250 °C in a

depth of 3–13 km for burial metamorphism in New Zealand. In contrast, Cho et al. [51] suggest 190 ± 30 °C for the Kartmutsen metabasites of Vancouver Island in Canada, and according to Kristmannsdottir [50] it is at about 200 °C in the high temperature hydrothermal fields in Iceland. The secondary minerals discussed here formed in the cavities of tholeiitic basalt, which never experienced burial of more than a few hundred meters, maximum. This environment is characterized by badly defined fluid pressure conditions and selective transport of distinct elements into the cavities. These facts must be kept in mind during the following discussion on the formation temperatures of the individual secondary minerals.

5.1.1. Minerals with Large Stability Fields

The minerals with large stability fields, and including greenschist facies conditions, are chlorite, quartz and calcite.

Chlorite, the first precipitated secondary mineral at Salsette Island, appears systematically in modeling results at low temperatures. In nature it is typical of greenschist facies conditions, but in hydrothermal environments formation is possible at as low as 200 °C (e.g., [50]).

Calcite is present in two generations. The first lamellar to platy calcite I crystals in the void spaces of the hyaloclastite breccia and the flat rhombohedral crystals in the pillow cavities are associated with laumontite, and both are characteristically completely overgrown by quartz or prehnite. Calcite II crystals with rhombohedral and scalenohedral forms were precipitated after quartz.

Patil et al. [52] studied the fluid inclusions of calcite from Salsette Island. They found significant differences in the homogenization temperatures for calcite developed in early veins and vesicles/cavities, respectively. The homogenization temperatures of the vein calcite are reported as being between 194 and 246 °C, and the temperatures in the cavities are reported at 161–178 °C. Unfortunately, they did not distinguish between calcite I and II crystals. However, Wise and Moller [39] studied Ca-Fe-silicates associated with calcite and noted homogenization temperatures of primary inclusions in the calcite of 180–195 °C. According to the observations presented here, calcite II is associated with Ca-Fe-silicates. To summarize, temperatures of 195–250 °C can be estimated for early formed calcite I, whereas calcite II developed at 160–195 °C.

Quartz occurs as macro crystalline crystals with only well-developed prisms, while microcrystalline and amorphous silica phases are absent. The formation of macro crystalline quartz in hydrothermal environments is promoted by temperatures >150 °C, low concentrations of silica in the solution, and the presence of electrolytes [50,53].

5.1.2. Minerals Typical for the Prehnite–Pumpellyite Facies

Currier [54], Wise and Moller [39] (Table 5), and Ottens [19] described several Fe-containing members of the prehnite–pumpellyite facies from Salsette Island, without referring to their relationships to the host rock and the crystallization sequence. With respect to the observations presented here, ilvaite and pumpellyite-(Fe²⁺) are present only in the pillow cavities, whereas babingtonite, julgoldite, and andradite occur in the void spaces of the hyaloclastite breccia, and prehnite occurs in both.

Julgoldite appears together with chlorite, prehnite, andradite, hematite, and quartz. While, Wise and Moller [39] described crystals from Mumbai as julgoldite-(Fe²⁺), Artioli et al. [55] and Nagashima et al. [56] concluded their investigations of Salsette specimens as julgoldite-(Fe³⁺).

Prehnite in the void spaces of the hyaloclastite displays an intensive green color, due to up to 4% Fe₂O₃ (up to 11 wt% FeO according to Wise and Moller [39]), while greyish to yellowish prehnite in the pillow cavities contains approximately 0.5% Fe₂O₃. The higher iron content in prehnite from the void spaces might be explained by the higher Fe content and fluid flow rate within the hyaloclastite breccia. An increase of the iron content with decreasing temperatures, as proposed by Weisenberger and Bucher [57], cannot be confirmed. In general, prehnite forms at temperatures >180–200 °C and <300 °C [48,58].

Table 5. Chemical composition (wt.%) of Ca-Fe-silicates from Salsette Island reported by Wise and Moller [39]. n.d.—not determined.

	Julgoldite-(Fe ²⁺)	Pumpellyite-(Fe ²⁺)	Ilvaite	Babingtonite	Andradite (OH) Bearing	Prehnite
SiO ₂	33.13	34.53	30.50	52.87	33.03	41.73
Al ₂ O ₃	2.99	11.84	0.15	0.51	2.25	15.71
FeO	33.03	22.42	51.32	21.29	35.96	11.16
MnO	0.04	0.13	0.77	0.84	0.05	-
MgO	1.41	1.44	0.60	1.96	0.31	-
CaO	20.72	21.65	14.40	20.10	33.78	26.21
l.o.ign.	n.d.	n.d.	n.d.	n.d.	n.d.	n.d.
Total	91.32	92.01	97.73	97.57	97.15	94.91

Babingtonite appears as intergrown with prehnite and quartz. The observations from Salsette Island correspond to those of Duggan [59], who studied the pillowed basalts in western Southland of New Zealand. He reports that babingtonite occurs as a common mineral in the void spaces between pillows, together with prehnite, pumpellyite, andradite, calcite, and quartz. It forms from hydrothermal solutions by direct precipitation in open spaces and by the replacement of higher temperature silicate phases in a shallow marine volcanic environment.

Ilvaite was deposited on calcite II crystals in the pillow cavities only. Considering the homogenization temperatures of fluid inclusions in calcite II (160–195 °C, Wise and Moller [39]), the formation temperature of ilvaite should also be less than 200 °C.

Pumpellyite-Fe⁽²⁺⁾ was only detected as crystals deposited on ilvaite. Wise and Moller [39] suggest that this precipitation sequence is due to increasing Ca and Al components in the fluid, causing formation of pumpellyite as a more stable phase. Based on this assumption, the formation temperature of pumpellyite is also expected to be about 180–200 °C.

5.1.3. Minerals of the Zeolite Facies

Zeolitization of basaltic rocks generally occurs in a temperature range from 40 to 250 °C in a water-rich environment (Table 6). Under open or closed system conditions, fresh volcanic glass is converted to palagonite, a microcrystalline and brownish to yellowish mixture of smectite, zeolites, and calcite. The zeolites may be subdivided into high- and low-temperature zeolites, which form above and below ca. 100 °C, respectively [50]. High-temperature zeolites include laumontite, yugawaralite, and wairakite, whereas typical low-temperature zeolites are mordenite, heulandite, stilbite, epistilbite, mesolite-scolecite, thomsonite, and chabazite. In Salsette Island, wairakite and thomsonite had not been reported until now. With the exception of the high-temperature zeolites, laumontite and yugawaralite, all other zeolites were discovered predominantly in the pillow cavities.

Laumontite is the dominant mineral of the zeolite facies of Salsette Island [37]. Microcrystalline laumontite occurs as layers, compact masses, or thin coatings, but centimeter-sized, transparent crystals were also found. With respect to its relationship to other phases, at least three generations can be distinguished. Laumontite I formed after chlorite but before the quartz wall lining. Laumontite II is present on top of quartz and overgrown by prehnite. Finally, laumontite III formed after prehnite. According to the literature, laumontite appears in a wide temperature range, from about 110 to 240 °C, coexisting with many other minerals (e.g., [48,50,60]). For the early laumontite I, the association with chlorite argues for temperatures up to 240 °C [60]. Laumontite II, including the large crystals, also formed at relatively high temperatures of >180 °C, at the transition or within the prehnite–pumpellyite facies. In contrast, Keith and Staples [61] argue for lower formation temperatures for cm-sized laumontite crystals formed at a late stage after mordenite in the Siletz River basalts, Oregon/USA. Temperatures of as low as 110 °C may be true for laumontite III.

Table 6. Estimated formation temperatures of zeolites and associated minerals of Salsette Island.

Mineral	Approx. Temp. °C	Temperature Range °C							
		300–250	250–200	200–150	150–100	100–90	90–70	70–50	<50
Chlorite	<300	————	—						
Calcite	100–300	————	————	————	————				
Babingtonite	200–250		————						
Yugawaralite	200–250		————						
Julgoldite	200–250		————						
Quartz	200–300	————	————	————					
Prehnite	>200	—	————						
Pumpellyite	<200			—					
Ilvaite	<200			—					
Laumontite	190–230		—	—					
Gyrolite	175–200			—					
Heulandite	120–150				—				
Epistilbite	100–130				—				
Stilbite	100–130				—				
Okenite	100–130				—				
Scolecite	90–100					—			
Natrolite	90–100					—			
Apophyllite	70–100				---	————	————		
Chabazite	50–70							————	
Gypsum	<50								—

Yugawaralite was deposited after laumontite I and quartz, together with babingtonite and before prehnite [19]. For yugawaralite from Iceland different formation temperatures can be found in the literature. Barrer and Marshall [62] expected a precipitation from hydrothermal fluids at temperatures of 270–350 °C, whereas Weisenberger and Selbekk [10] proposed temperatures of about 110 °C based on field mapping and because yugawaralite had formed in the same mineralization stage as laumontite. The temperature stability field of yugawaralite is considered to be intermediate between that of laumontite and wairakite [63,64]. Experimental studies by Zeng and Liou [65] define an invariant point (234 °C, 550 bars where $P_{H_2O} = P_{total}$), where yugawaralite, wairakite, and laumontite are stable. The absence of wairakite in Salsette samples indicates lower temperatures.

The zeolites, heulandite-Ca, stilbite-Ca, and epistilbite occur rather rarely. They developed after calcite II in the pillow cavities in the temperature range 80–160 °C [50,66].

Chabazite-Ca is a rare zeolite in Salsette Island [19]. The crystals were not overgrown by other minerals and belong to the latest formations, probably at 40–80 °C [60]. Several chemical analyses of chabazite resulted in up to 1.40% Na and 1.02% K at corresponding Ca contents of 8.02%. The Na end member gmelinite was not detected.

Natrolite is interesting when considering the question of whether seawater could have an influence on the chemical composition of the secondary minerals from Salsette Island. It was found only rarely in the pillow cavities, as the latest epitaxial overgrowth on scolecite. Occasionally it is associated with Na bearing stilbite. The later precipitated chabazite-Ca also contains Na. However, the sodium content of these three minerals seems not to be a significant indication of the influence of seawater, because the Na bearing minerals occur in the selvedge protected pillow cavities but are missing in the void spaces of the surrounding hyaloclastite breccia.

5.1.4. Hydrated Calcium Silicate Minerals

The hydrated calcium silicates gyrolite and okenite belong to the most characteristic and commonly occurring minerals in Salsette Island and are more frequently found in cavities of the pillows than in void spaces.

Merlino [67] stated that the crystal lattice of natural gyrolite always contains both Na and Al, and the most likely composition of natural gyrolite is $\text{NaCa}_{16}\text{Si}_{23}\text{Al}_{60}(\text{OH})_{8}\cdot 14\text{H}_2\text{O}$. The analysis of the gyrolite from Salsette Island resulted in 2.21 wt% Al_2O_3 and 0.26 wt% Na_2O , confirming this observation. The green-brown coloration of some gyrolite is most likely due to the substitution of Ca by Fe and Mn [37,68,69]. Baltakys and Siauciunas [70] describe the experimental synthesis of gyrolite at temperatures of 175 °C to 200 °C, and they point out that gyrolite only rarely occurs together with zeolites. As gyrolite was precipitated later than calcite II (formed at 160–195 °C), temperatures close to 175 °C seem likely.

Okenite was formed as the latest calcium silicate in Salsette Island. A late formation is indicated by a second generation of microscopic okenite crystals rarely occurring on apophyllite in the void spaces of the hyaloclastite breccia. Kurnosov [71] attributed okenite to a group of ‘middle-temperature minerals’ formed at 100–350 °C. However, Taylor [72] stated that synthesis of okenite is possible only at low temperatures, a little above or perhaps even below 100 °C.

5.1.5. Apophyllite

Apophyllite from Salsette Island can be characterized as an intermediate member of fluor- and hydroxyapophyllite-(K) [73]. With the exception of gypsum and the second okenite generation, apophyllite is the latest secondary mineral precipitated. The crystals are commonly colorless, and only a very limited number of pale greenish crystals have been observed. With respect to other occurrences from the main DVP, the green color is due to a V content of several hundred ppm [46,74]. Information on the formation temperature of apophyllite is rare. For late formed fluorapophyllite-K crystals from the main DVP, temperatures of 141–222 °C [14] or alternatively 250–280 °C [75] were reported based on fluid inclusion homogenization temperatures. In contrast, fluorapophyllite-(K) formed at 70–100 °C in veins of the Swiss Alps together with laumontite and quartz [76]. According to these data, formation temperatures in the wide range of 70–150 °C can be estimated.

Rb-Sr ages of apophyllite determined from a pillow cavity (sample K4a) and a void space of the hyaloclastite breccia (sample BOM-3) were about 40 Ma and 30 Ma, respectively. The K-Ar age of the latter sample is 27 Ma and, therefore, slightly younger than the Rb-Sr age. At first glance, these data seem to be a bit erratic, but in comparison to other literature data, they are geologically meaningful. As discussed in Ottens et al. [14], Rb-Sr ages are typically a bit higher than the corresponding K-Ar or Ar-Ar ages measured on the same sample material. Furthermore, apophyllite always forms with a significant time lag, with respect to the eruption of the host volcanic rocks and the ages may scatter in a range of several million years, even in the same lava flow. The differing timing of crystallization is explained by heterogeneously distributed hydrothermal fluids, which are present over extended time periods (e.g., [14,77,78]). For example, in the main DVP they are in the range of 20–60 Ma, and even in the locality of Savda/Jalgaon they yield ages in the range of 28–44 Ma [14].

5.1.6. Ore Minerals

The observed ore minerals include the sulfides pyrite, chalcopyrite, sphalerite, and galena, and the oxides hematite and ferberite. While hydrothermal mobilization of Fe, Cu, Zn, and Pb from basaltic rocks is very common, the occurrence of well-developed ferberite crystals [79] is remarkable, as the W content of the tholeiites is very low at 1 ppm or less [80].

5.2. Aspects of the Fluid Conditions

The precipitation of the secondary minerals was controlled by fluids, which, therefore, give information on the physical conditions and the chemical composition of the latter.

Based on the observed secondary minerals and their precipitation sequence, decreasing temperatures and Fe contents in the fluid are indicated. A limited silica concentration can be deduced by the occurrence of quartz instead of amorphous silica minerals. Furthermore, differences in both the fluid circulation in the interpillow matrix and hyaloclastite breccia, and in the interior of the pillows can be expected.

5.2.1. Fluid Conditions in the Interpillow Void Spaces

The hyaloclastite breccia is characterized by high porosity and permeability. It will have been saturated by fluid immediately after the eruption and stayed as an open system for a long time. The number of secondary mineral species and their volume varies significantly between individual void spaces, which may be due to the heterogeneous flow capacity. Since they do not show any systematics with respect to their position in the void spaces, the latter will have been completely filled with a homogeneous fluid during any times of precipitation.

Larger masses and crystals of laumontite and large aggregates of prehnite indicate a high material turnover in the early phase of cooling, in the temperature range of 200 to 250 °C. Interestingly, some typical low temperature zeolites such as heulandite, stilbite, epistilbite, natrolite/scolecite, and chabazite are absent in the void spaces.

5.2.2. Fluid Conditions in the Pillow Cavities

The spilitic basalt forming the pillows has a low permeability and exhibits a heterogeneously distributed alteration. Nevertheless, most of the cavities were in a limited exchange with the interpillow matrix via cracks. As the cracks have been filled by laumontite and calcite, the cavities have, at least temporarily, represented a more or less closed system, with limited fluid immigration. Generally, the pillow cavities are only partly filled by secondary minerals, and the volume or weight of the precipitated secondary minerals seems to be somehow related to the volume and surface of the cavity space. The early precipitated minerals chlorite, calcite I, laumontite I, quartz, and calcite II occur all around the cavity walls, without any preferred orientation, whereas later formed minerals such as okenite tentatively appear on the bottom or side of the cavities. This implies that the cavities had been completely filled by a homogeneous fluid during the early stage of mineralization, but that later on the conditions might have changed.

In this context, the mineralized crusts, which have been observed occasionally, are of special interest. The crusts in the pillow cavities are 0.5–3 mm thick and commonly consist of calcite with a brownish centerline, caused by contamination of clay minerals (pers. com. Pöhlmann, 1996) and an overgrowth by quartz. However, mostly broken pieces of crust are present at the bottom of the cavities, forming clusters encrusted and welded by quartz and other minerals (Figure 7b). Crusts from the void spaces in the Kurar quarry show big quartz crystals formed on the bottom side, whereas small ones appear on the upper side (Figure 8e2). This indicates different conditions below and above the crust at least during part of the time.

The crusts most likely formed horizontally, orientated on top of the surface of a solution, partly filling the cavities and void spaces. This solution may represent condensed fluid mixed with infiltrated water. Interestingly, crusts are not present in most cavities, and in some cases several levels are present in the same blister cavity. This might be due to heterogeneity of the fluid and a partial drainage of the solution. Most observed crusts collapsed, but the reason for the collapse can only be speculated. They most likely broke under their own weight. However, it is also possible that boiling of the solution during the reheating in the course of increasing temperature caused the collapse. Unfortunately, there is no information as to whether the crusts were found in an absolutely horizontal position or whether they displayed a dipping of ~15° analogous to the greater Salsette subgroup succession [6]. Such observations would provide additional evidence for the timing of the precipitation of the secondary minerals.

5.3. Geological Setting

The Salsette subgroup represents the last phase of the DVP and erupted in early Paleocene time, at around 62.5 to 60.5 Ma. At the time of the magmatic activity, India drifted northward towards Asia at a rate of about 15 cm per year. At its western margin, it was affected by rift processes in the course of the India–Laxmi Ridge–Seychelles breakup [6]. The greater Mumbai area was located at a paleo coastline with lagoons, at least partly with a brackish to freshwater environment [8,35]. Most of the volcanic rocks extruded subaqueously, forming pillows and pyroclastics, as well subaerial massive lava flows [17]. Contact with brackish or fresh water is supported by the observed secondary minerals in Salsette Island. In general, they are dominated by Na-poor varieties, and Na-rich zeolites, such as analcime, gmelinite, lévyne, mordenite, and thomsonite, typical for pillows formed in a marine environment [81], are absent in Salsette. According to Subbarao [47], the Sr-isotopic composition of the spilite from Bhoiwada also shows no influence of contamination by a component with Paleogene seawater values.

The pillowed basalt is exposed in the studied quarries at an elevation of 20–65 m asl and in the Dahisar River bed to about 80 m asl. Duraiswami et al. [17] assumed, based on the similar composition to the unspilitized parts of the Bhoiwada lava unit (South Mumbai) [47], that the Borivali (Dahisar River bed) pillows belong to the same lava flow, indicating a common emplacement history. It was also assumed that the pillows from the studied Salsette quarries and those from the Dahisar River bed belong to a common pillow flow field, but formed different morphologies and textures depending on the position in this flow field and their cooling histories. The morphology of the pillow flows in the quarries could only be assessed to a limited extent. Longitudinal tubes, as pronounced in the Dahisar River bed (Figure 2b), could not be observed. The ellipsoidal shapes point to the formation of single pillows, which were located on more or less steep slopes. This also explains the occasional embedding in hyaloclastic breccia. The cavities have a largely round and flattened shape, are enclosed on all sides by the pillow matrix, and are classified as former gas blisters or drained cavities. The pillows in the Dahisar River bed have a significantly denser texture, and cavities are missing [17], which also resulted in less spilitic alteration and mineralization. As the Dahisar river bed pillows are fresh and only slightly altered, they are likely to have been in an area of lava flow that had limited alteration and spilitization in contact with water. The pillows of the quarries indicate intensive spilitization and alteration, which points to a marginal position in the lava flow under water. The assumption that the dark spots in the spotted rock are fresh, non-spilitized basalt is based on reports by Sethna and Javeri [82] and Naik et al. [83]. Studies of other spotted rocks in the Thane–Vasai region resulted that the spotted rocks are formed by incomplete quenching of basaltic lavas during their entry into streams or shallow freshwater lakes [30]. The different assessments are to be regarded as an open puzzle.

Due the high homogenization temperatures of the fluid inclusions in calcite, Wise and Moller [39] suggested a burial depth of more than 1000 m but less than 2000 m for the pillow basalts at Salsette Island. However, such a burial can be ruled out, because the eruptions of the Salsette subgroup belonged to the latest phase of the DVP, and no overlying sedimentary piles are known, except minor quaternary deposits. The tholeiitic succession exposed in the studied quarries is only overlain by thin tholeiitic sheet layers and by younger explosive volcanics with trachytic to rhyolitic composition [16,29]. Furthermore, some later dioritic intrusions occur at short distances of a few hundred meters up to a few km from the studied quarries [31]. The younger magmatic rocks will have produced local heat domes, which may have been crucial for the further alteration of the tholeiitic basalts and the precipitation of secondary minerals in the cavities. Parts of the secondary minerals and the calcite with the studied fluid inclusions therein most likely formed from such hot hydrothermal fluids. Similar processes have been described in other localities, e.g., by Keith and Staples [61] for the Siletz River volcanics (Coast Range, OR, USA), or by Westercamp [84] for Martinique Island.

Today the volcanic sequence is dipping about 15° to the west. Pillows are exposed between ~20 to 80 m asl, and the overlying volcanoclastics up to 200 m asl near to the Kanheri caves (Figure 2a). Assuming uplift of the area as a whole block, a water column of about 200 m on top of the lowermost outcrops would be indicated. However, such a water depth is unlikely in a brackish or fresh water lagoonal environment. The recent situation would have been the result of sea level drop after the high eustatic sea level during the early Paleocene time (61.8–62.9 Ma) [17], in combination with syn-rift tilting and domino-type block-faulting and post-rift regional uplift of the western Deccan Traps. According to the latter authors, the deformation of the Panvel flexure zone occurred in a short time interval around 62.5 Ma [24], contemporaneous to the late stages of magmatism. This is well documented, e.g., on Elephanta Island just south-east of greater Mumbai [6].

The uplift of the volcanic sequence above sea level is most probably related to the rifting event. It would have had an influence on the fluid system. The brackish water of the lagoon could have been partially drained, and at the same time meteoric water could have flowed in. It is possible that the change, from cavities completely filled with fluid, to cavities only partially filled with a solution, is related to the regional uplift. Reheating and the establishment of a new fluid system was possibly due to the nearby intrusions of the ongoing magmatic activity.

The tectonic and magmatic activity in the area stopped while still in Danian time, and since, the western margin of India formed a passive continental margin [24]. The overburden was limited and, therefore, only very low temperature mineralization would be expected. All the more astonishing is the formation of apophyllite in the period between 30 and 40 Ma. Apophyllite is overgrown partly by okenite, and the minimum formation temperatures can be estimated to be about 70°C [76]. The only possible explanation is a new pulse of hydrothermal fluids in the late Eocene to earliest Oligocene, even if there are no hints at this from the regional geology. However, the data from the main DVP [14] point in the same direction.

5.4. Summarizing Genetic Model for the Secondary Minerals of Salsette Island

During their eruption, the tholeiitic lavas of the Salsette subgroup came into contact with brackish or fresh water in a shallow lagoonal environment. This caused rapid cooling and the formation of pillow structures, accompanied with spilitic alteration and formation of hyaloclastite and pillow breccia. Void spaces of the breccia were immediately filled by fluid, which was heated up and also migrated into the pillow cavities via cracks. In the beginning, the fluid interacted mostly with volcanic glass and was mineralized, mainly by SiO_2 , Al_2O_3 , Fe_2O_3 , MgO , CaO , and minor Na_2O . During this initial cooling, chlorite, laumontite I, quartz, and calcite I formed. Temperatures decreased to below 200°C or even 100°C , probably causing condensation of the fluid in several of the pillow cavities (Figure 10).

Shortly thereafter, ongoing magmatic activity produced more acidic volcanics and nearby intrusions. These are probably responsible for the reheating and activation of the hydrothermal system. Further decomposition of the volcanic glass supplied the same components into the fluid as before, and a second phase of mineral precipitation occurred in a temperature range of $180\text{--}270^\circ\text{C}$, corresponding to the prehnite–pumpellyite facies. Besides calcite and quartz, some Fe- and Mg-bearing silicate minerals, as well as high temperature zeolites, were formed. Based on the study of hand specimens, the general precipitation sequence was babingtonite, laumontite II, prehnite, julgoldite, yugawaralite, calcite II, ilvaite, pumpellyite, and gryolite. This sequence is again compatible with a decreasing temperature trend. However, modifications might be due to fluctuating temperature and changes in the fluid composition. Such changing conditions are able to explain the formation of the perimorphs and casts of prehnite after laumontite, present in the void spaces of the hyaloclastite breccia. The significantly higher mineral formation in the void spaces of the hyaloclastite with respect to the pillow cavities can be explained by a higher fluid interaction and stronger alteration of the surrounding material.

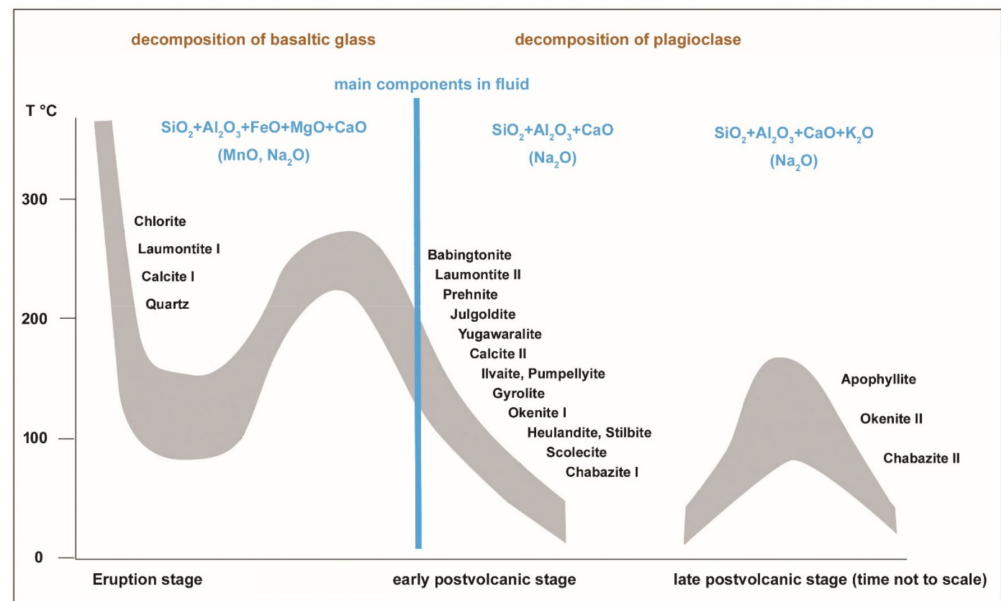


Figure 10. Estimated theoretical model of mineral formation in the pillowed basalt on Salsette Islands: During the eruption stage, interaction of hot lava with water resulted in extensive alteration and formation of chlorite, laumontite I, calcite I, and quartz. After a short period of more or less cooling down, reheating in an early postvolcanic stage up to ca. 300 °C was again followed by successive cooling and temperature controlled precipitation, beginning with minerals of prehnite-pumellyite facies and followed by zeolites. In a later postvolcanic stage several million years after eruption, formation of apophyllite, okenite II, and chabazite II occurred at significantly lower temperature.

Further temperature decreases, from ca. 180 °C to less than 100 °C, led to zeolite facies conditions. Okenite I, scolecite, heulandite, stilbite, and, finally, chabazite I formed. The chemical composition of the zeolites, which contain no Fe_2O_3 and MgO , indicates mineralization from magmatic plagioclase. The low-temperature zeolites only formed in the pillow cavities and often occur in the bottom part of them. It is likely that magmatism terminated and the Salsette subgroup was above sea level and infiltrated by meteoric water during this phase. Possibly, some of the void spaces in the hyaloclastite breccia were dry, at least temporarily, and maybe the cavities were filled only partly by a solution at temperatures below 100 °C. There are no Cenozoic transgressional sequences overlying the Salsette subgroup, and, therefore, it has probably stayed above sea level since the end of the magmatic activity at 60.5 Ma. There have also been no known tectonic events, which could explain the new phase of hydrothermal activity indicated by the formation of apophyllite, okenite, and chabazite II. They formed in the late Eocene to earliest Oligocene 20 to 30 Ma, after the end of the Deccan volcanism. Temperatures for the corresponding fluids will have been at a minimum of 50 °C, but might have reached up to more than 100 °C.

5.5. Comparison to the Main DVP and Other Occurrences Worldwide

In this chapter, the mineralization described above is compared to a very similar deposit a little further north, then to the main part of the DVP in the east, and finally to some other localities worldwide.

5.5.1. Secondary Minerals of the Daman Area

Near Daman (20°12'–20°30' N and 72°49'–73° E), approximately 130 km north of Mumbai and at an altitude of 100–200 m above sea level, a quite similar sequence of spilitized basalt is present. It mostly consists of hyaloclastite breccia, and more rarely basalts with pillow structures [82,85]. The pillows contain vesicles filled completely by zeolites, chlorite, and calcite, and in some cases by quartz. Very rarely open cavities

with idiomorphic crystals of laumontite, calcite, quartz, and apophyllite have been found. Zeolites and calcite appear as secondary minerals in the highly altered hyaloclastite.

5.5.2. Comparison to the Secondary Minerals of the Main DVP

The assemblage of secondary minerals in the main DVP shows remarkable differences in comparison to Salsette Island. A detailed study on the precipitation sequence focusing on the quarry complex of Jalgaon/Savda and the Nashik area was recently published by Ottens et al. [14]. The authors argue for a complex scenario, with several phases of precipitation between 65 and 20 Ma and fluctuating temperatures. In comparison, the following differences are obvious:

Chlorites do not occur in the vesicles and cavities of the main DVP, where the alteration took place at lower temperatures, resulting in the formation of celadonite and smectites, among others [14].

Instead of macrocrystalline quartz, chalcedony is the most frequent SiO₂ variety in the MDP, even if the formation runs through several structural states of SiO₂ with amorphous silica as its first solid phase and macrocrystalline quartz later on [14].

Fe-bearing minerals typical for the prehnite–pumpellyite facies (e.g., prehnite, pumpellyite, ilvaite, etc.) are absent in the main DVP. The only exception is julgoldite-(Fe²⁺), which was observed in the quarry complex of Jalgaon/Savda as pseudomorphs after mordenite [69].

Laumontite has been observed even less frequently in several localities in the main DVP. In the Nashik area it commonly appears before and after stilbite, scolecite, and apophyllite [69]. Additionally, laumontite was observed near Soygaon in the Aurangabad district as unusual clusters, partially developed on apophyllite [86].

Scolecite is the most common zeolite of the natrolite sub-group in the main DVP, whereas natrolite has been detected very rarely until now [12,36,46,68,87].

In contrast to Salsette Island, the zeolites heulandite-Ca, stilbite-Ca, and epistilbite represent the most common secondary minerals in the main DVP [12,36,46]. They formed in vesicles and large cavities [14]. In addition, chabazite-Ca, gyrolite, and okenite are much less common in the main DVP [19].

Fluorapophyllite-(K) belongs to the most common secondary minerals in the main DVP, where it develops large crystals of up to 10 cm in a wide variety of associations, shapes, and occasionally with an intense green color, due to an elevated V content.

Ore minerals such as sulfides or oxides and Ca-Fe-silicates are unknown or very rare in the main DVP. Hematite was observed as tiny 1-mm-sized spheres on fluorite and goethite as crystals up to 2 mm near Sinnar/Mohadari [46]. Flakes of native copper were recently found in the Wagholi quarries near Pune (pers. comm. Makki, 2019).

Some minerals occurring only occasionally in the main DVP, e.g., powellite or cavansite, are missing on Salsette Island. Additionally, biogenic structures, such as those described from the quarry complex of Jalgaon/Savda [88], have not been known until now in the Salsette Islands.

5.6. Comparison with the Secondary Minerals from Other Pillowed Basalts

Pillow basalts are some of the most abundant rocks on earth [89], but most of them form in a marine environment. The number of similar deposits that have been studied in detail and can be used for comparison are very limited.

The Siletz River volcanics in Oregon and the Watchung basalts in New Jersey belong to such occurrences, but are also characterized by significantly different features. The Siletz River volcanics represent early Eocene subaqueous flows of tholeiitic basaltic pillow lavas and breccia deposited in a shallow, constantly subsiding basin [61]. The emplacement, alteration, and mineralization conditions show some similarities to Salsette Island. As minerals of the prehnite–pumpellyite facies do not occur [61], most of the secondary minerals in the Siletz River volcanics formed at less than 150 °C.

The Watchung basalts in New Jersey are well known for their abundant well-developed crystals of secondary minerals. Pillow structures occur only sporadically. According to

the section at the Watchung Ridges, the basaltic flows are under-, inter-, and overlain by sediments [90–92]. The mineral specimens described by Mason [91], and Laskowich and Puffer [92], were found in the second Watchung flow ‘extruded by fissures eruptions into a shallow brackish lake water’. This is partly comparable to Salsette Island, but there are remarkable differences in the observed minerals. Spilitization is not reported for the Watchung basalt, and Na-rich minerals such as gmelinite and pectolite or sulfates such as anhydrite and glauberite occur.

6. Conclusions

1. The secondary minerals were deposited in the early Paleocene time (62.5 to 61.5 Ma) Salsette subgroup, which represents the youngest part of the Deccan Volcanic province. The host rocks are partly spilitized tholeiitic basalts, with pillow structure and hyaloclastic interpillow breccia, which formed when the lava came into contact with brackish and fresh water of a lagoonal environment.
2. Secondary minerals developed in pillow cavities and in void spaces of the hyaloclastic interpillow matrix. The two positions show distinctly different secondary mineralization, due to differences in fluid activity. The highly permeable interpillow matrix formed an open system, whereas the pillow cavities became more or less closed systems, at least temporarily.
3. The mineral species indicate formation through interaction of the rock with fresh water. Minerals characteristic of the influence of seawater have not been observed.
4. Precipitation can be subdivided into three stages:
 - 4.1. During initial cooling after the eruption at about 62 Ma chlorite, laumontite I, quartz, and calcite I developed.
 - 4.2. Due to reheating caused by ongoing magmatic activity, the second stage of precipitation started at prehnite–pumpellyite facies conditions. With decreasing temperatures, in the range of 270–180 °C, babingtonite, laumontite II, prehnite, julgoldite, yugawaralite, calcite II, ilvaite, pumpellyite, and gryolite developed. Ongoing temperature decreases caused zeolite facies conditions, and okenite I, scolecite, heulandite, stilbite, and, finally, chabazite I were precipitated in the temperature interval of 180 °C to less than 100 °C. During the first stage and the beginning of the second stage, the fluid contained $\text{SiO}_2 + \text{Al}_2\text{O}_3 + \text{FeO} + \text{MgO} + \text{CaO}$, and minor MnO and Na_2O , whereas later on FeO and MgO were absent.
 - 4.3. According to Rb-Sr and K-Ar data on apophyllite, a third stage of precipitation occurred in the late Eocene to early Oligocene (30–40 Ma). Besides apophyllite, okenite II and chabazite II formed. Significant amounts of K_2O are only indicated by the formation of apophyllite-K in the third stage.

Author Contributions: B.O. collected the studied samples. The authors B.O., R.S. and Z.B. conducted different analytical measurements. B.O. and R.S. evaluated the mineralogical and geochemical data and wrote the manuscript. All authors have read and agreed to the published version of the manuscript.

Funding: This research received no external funding.

Data Availability Statement: Not applicable.

Acknowledgments: This manuscript was greatly improved by the thorough and critical pre-reviews by Raymond A. Duraiswami and Sam F. Sethna, The authors would also like to thank Jens Götze and the two anonymous reviewers for the critical and insightful reading and comments. Thanks to Salim Tyebjee and Hemant Merchant for their support and hospitality during sampling. We are grateful to Erich Keck for RFA and XRD analysis, and Monika Horschinegg for her help performing the Rb-Sr measurements at the University of Vienna. K/Ar analyses were supported by the János Bolyai Scholarship of the Hungarian Academy of Sciences to Zsolt Benkó. Thanks also to Stephan Wolfsried, László Kupi, and Giovanni Ciccolini for photographs and to Katherine Wilson for her help in revising the English style.

Conflicts of Interest: The authors declare no conflict of interest.

References

1. Walker, G.P.L. Some observations and interpretations on the Deccan traps. *Mem. Geol. Soc. India* **1969**, *43*, 367–395.
2. Pande, K. Age and duration of the Deccan Traps, India: A review of radiometric and paleomagnetic constraints. *J. Earth Planet. Sci.* **2002**, *111*, 115. [[CrossRef](#)]
3. Sheth, H.C. Deccan Volcanism: Recent Indian Research. In *Glimpses of Geoscience Research in India: The Indian, Report to IUGS 1999–2004*; Singhvi, A.K., Bhattacharya, A., Eds.; The Indian National Science Academy (INSA): New Delhi, India, 2004; pp. 19–25.
4. Sheth, H.C.; Zellmer, G.F.; Demonterova, E.I.; Ivanov, A.V.; Kumar, R.; Patel, R.K. The Deccan tholeiite lavas and dykes of Ghatkopar-Powai area, Mumbai, Panvel flexure zone: Geochemistry, stratigraphic status, and tectonic significance. *J. Asian Earth Sci.* **2014**, *84*, 69–82. [[CrossRef](#)]
5. Kumar, A.; Pal, S.; Shrivastava, J.P. Contemporary researches and issues related to the Deccan volcanism. *Proc. Indian Natl. Sci. Acad.* **2020**, *86*, 49791. [[CrossRef](#)]
6. Patel, V.; Sheth, H.; Cucciniello, C.; Joshi, G.W.; Wegner, W.; Samant, H.; Sen, B.; Koeberl, C. Geochemistry of Deccan Tholeiite Flows and Dykes of Elephanta Island: Insights into the Stratigraphy and Structure of the Panvel Flexure Zone, Western Indian Rifted Margin. *Geosciences* **2020**, *10*, 118. [[CrossRef](#)]
7. Sukheswala, R.N.; Avasia, R.K.; Gangopadhyay, M. Observations on the occurrence of secondary minerals in the Deccan Trap of Western India. *Ind. Mineral.* **1972**, *13*, 50–68.
8. Sukheswala, R.N. Gradation of tholeiitic Deccan basalt into spilite, Bombay, India. In *Spilites and Spilitic Rock*; Amstutz, G.C., Ed.; Springer: Cham, Switzerland, 1974; pp. 229–250.
9. Neuhoff, P.S. Porosity evolution and mineral paragenesis during low-grade metamorphism of basaltic lavas at Teigarhorn, eastern Iceland. *Am. J. Sci.* **1999**, *299*, 467–501. [[CrossRef](#)]
10. Weisenberger, T.; Selbekk, R.S. Multi-stage zeolite facies mineralization in the Hvalfjörður area, Iceland. *Int. J. Earth Sci.* **2008**, *98*, 985–999. [[CrossRef](#)]
11. Mattioli, M.; Cenni, M.; Passaglia, E. Secondary mineral assemblages as indicators of multistage alteration processes in basaltic lava flows: Evidence from the Lessini Mountains, Veneto Volcanic Province, Northern Italy. *Periodico di Mineralogia* **2016**, *85*, 1–24. [[CrossRef](#)]
12. Jeffery, K. Mineral Chemistry of Zeolites from the Deccan Basalts. Ph.D. Thesis, Royal Holloway and Bedford New College, University of London, London, UK, 1988. Published by ProQuest LLC (2016).
13. Sabale, A.B.; Vishwakarma, L.L. Zeolites and associated secondary minerals in Deccan volcanics: Study of their distribution, genesis and economic importance. National Symposium on Deccan Flood Basalts, India, Gondwana. *Geol. Mag.* **1996**, *2*, 511–518.
14. Ottens, B.; Götz, J.; Schuster, R.; Krenn, K.; Hauzenberger, C.; Zsolt, B.; Vennemann, T. Exceptional Multi Stage Mineralization of Secondary Minerals in Cavities of Flood Basalts from the Deccan Volcanic Province, India. *Minerals* **2019**, *9*, 351. [[CrossRef](#)]
15. Sethna, S.F. Geology around Bombay—Some Intriguing Problems. *Mem. Geol. Soc. India* **1981**, *10*, 87–92.
16. Sethna, S.F. Geology of Mumbai and Surrounding Areas and its Position in the Deccan Volcanic Stratigraphy, India. *J. Geol. Soc. India* **1999**, *53*, 359–365.
17. Duraiswami, R.A.; Jutzeler, M.; Karve, A.V.; Gadpallu, P.; Kale, M.G. Subaqueous effusive and explosive phases of late Deccan volcanism: Evidence from Mumbai Islands, India. *Arab. J. Geosci.* **2019**, *12*, 703. [[CrossRef](#)]
18. Ottens, B. Seltene Mineralien aus dem indischen Basalt. *Lapis* **1988**, *4*, 32–33.
19. Ottens, B. Die Drusenmineralien aus dem Spilitbasalt von Bombay/Indien. *Der Aufschluss* **1998**, *49*, 133–149.
20. Self, S.; Widdowson, M.; Thordarson, T.; Jay, A. Volatile fluxes during flood basalt eruptions and potential effects on the global environment: A Deccan perspective. *Earth Planet. Sci. Lett.* **2006**, *248*, 518–532. [[CrossRef](#)]
21. Chenet, A.-L.; Courtillot, V.; Fluteau, F.; Gérard, M.; Quidelleur, X.; Khadri, S.F.R.; Subbarao, K.V.; Thordarson, T. Determination of rapid Deccan eruptions across the Cretaceous-Tertiary boundary using paleomagnetic secular variation: 2. Constraints from analysis of eight new sections and synthesis for a 3500-m-thick composite section. *J. Geophys. Res. Space Phys.* **2009**, *114*, 6103. [[CrossRef](#)]
22. Keller, G.; Sahni, A.; Bajpai, S. Deccan volcanism, the KT mass extinction and dinosaurs. *J. Biosci.* **2009**, *34*, 709–728. [[CrossRef](#)]
23. Sprain, C.J.; Renne, P.R.; Vanderkluyzen, L.; Pande, K.; Self, S.; Mittal, T. The eruptive tempo of Deccan volcanism in relation to the Cretaceous-Paleogene boundary. *Science* **2019**, *363*, 866–870. [[CrossRef](#)]
24. Pande, K.; Yatheesh, V.; Sheth, H. ⁴⁰Ar/³⁹Ar dating of the Mumbai tholeiites and Panvel flexure: Intense 62.5 Ma onshore-offshore Deccan magmatism during India-Laxmi Ridge-Seychelles breakup. *Geophys. J. Int.* **2017**, *210*, 1160–1170. [[CrossRef](#)]
25. Ganerød, M.; Torsvik, T.H.; van Hinsbergen, D.; Gaina, C.; Corfu, F.; Werner, S.; Owen-Smith, T.; Ashwal, L.D.; Webb, S.J.; Hendriks, B.W.H. Palaeoposition of the Seychelles microcontinent in relation to the Deccan Traps and the Plume Generation Zone in Late Cretaceous-Early Palaeogene time. *Geol. Soc. Lond. Spec. Publ.* **2011**, *357*, 229–252. [[CrossRef](#)]
26. Duraiswami, R.A.; Gadpallu, P.; Shaikh, T.N.; Cardin, N. Pahoehoe-a'a transitions in the lava flow fields of the western Deccan Traps, India-implications for emplacement dynamics, flood basalt architecture and volcanic stratigraphy. *J. Southeast Asian Earth Sci.* **2014**, *84*, 146–166. [[CrossRef](#)]
27. Kale, V.; Bodas, M.; Chatterjee, P.; Pande, P.C.A.K. Emplacement history and evolution of the Deccan Volcanic Province, India. *Episodes* **2020**, *43*, 278–299. [[CrossRef](#)]
28. Duraiswami, R.A.; Sheth, H.; Gadpallu, P.; Youbi, N.; Chellai, E.H. A simple recipe for red bole formation in continental flood basalt provinces: Weathering of flow-top and flow-bottom breccias. *Arab. J. Geosci.* **2020**, *13*, 953. [[CrossRef](#)]

29. Sheth, H.C.; Pande, K. Geological and $^{40}\text{Ar}/^{39}\text{Ar}$ age constraints on late-stage Deccan rhyolitic volcanism, inter-volcanic sedimentation, and the Panvel flexure from the Dongri area, Mumbai. *J. Southeast Asian Earth Sci.* **2014**, *84*, 167–175. [[CrossRef](#)]
30. Naik, A.; Sheikh, J.M.; Sheth, H.; Samant, H.; D'Souza, S. Diverse late-stage (≤ 62.5 Ma) Deccan volcanism and plutonism in the Thane–Vasai region, Panvel flexure zone, western Indian rifted margin. *J. Earth Syst. Sci.* **2021**, *130*, 152. [[CrossRef](#)]
31. Sheth, H.C.; Pande, K.; Bhutani, R. ^{40}Ar - ^{39}Ar ages of Bombay trachytes: Evidence for a Palaeocene phase of Deccan volcanism. *Geophys. Res. Lett.* **2001**, *28*, 3513–3516. [[CrossRef](#)]
32. Zellmer, G.F.; Sheth, H.C.; Iizuka, Y.; Lai, Y.-J. Remobilization of granitoid rocks through mafic recharge: Evidence from basalt-trachyte mingling and hybridization in the Manori–Gorai area, Mumbai, Deccan Traps. *Bull. Volcanol.* **2012**, *74*, 47–66. [[CrossRef](#)]
33. Sethna, S.F.; Merchant, H. Differentiation of the Deccan trap basalt flow in Bombay Island. *J. Geol. Soc. India* **1976**, *17*, 370–379.
34. Merchant, H. Structural Geology and Petrology of the Island Bombay and Surrounding Areas. Ph.D. Thesis, Bombay University, Mumbai, India, 1977, (unpublished).
35. Cripps, J.; Widdowson, M.; Spicer, R.; Jolley, D. Coastal ecosystem responses to late stage Deccan Trap volcanism: The post K–T boundary (Danian) palynofacies of Mumbai (Bombay), west India. *Palaeogeogr. Palaeoclim. Palaeoecol.* **2005**, *216*, 303–332. [[CrossRef](#)]
36. Wilke, H.J. Die Drusenminerale der westindischen Basalte. *Lapis* **1984**, *9*, 9–27.
37. Wise, W.S. Yugawaralite from Bombay, India. *Mineral. Rec.* **1978**, *5*, 296.
38. Meyer, I. Gyrolith, Die verschiedenen Färbungen und Ursachen. *Lapis* **1982**, *7*, 14–16.
39. Wise, W.S.; Moller, W.P. Occurrence of Ce-Fe-silicate minerals with zeolites in basalt cavities at Bombay, India. *Eur. J. Mineral.* **1990**, *2*, 875–883. [[CrossRef](#)]
40. Sölva, H.; Grasemann, B.; Thöni, M.; Thiede, R.; Habler, G. The Schneeberg Normal Fault Zone: Normal faulting associated with Cretaceous SE-directed extrusion in the Eastern Alps (Italy/Austria). *Tectonophysics* **2005**, *401*, 143–166. [[CrossRef](#)]
41. Vermeesch, P. IsoplotR: A free and open toolbox for geochronology. *Geosci. Front.* **2018**, *9*, 1479–1493. [[CrossRef](#)]
42. Balogh, K. K/Ar dating of Neogene volcanic activity in Hungary: Experimental technique, experiences and methods of chronological studies. *ATOMKI Közlemenyek* **1985**, *27*, 277–288.
43. Nier, A.O. A Redetermination of the Relative Abundances of the Isotopes of Carbon, Nitrogen, Oxygen, Argon, and Potassium. *Phys. Rev.* **1950**, *77*, 789–793. [[CrossRef](#)]
44. Steiger, R.; Jäger, E. Subcommittee on geochronology: Convention on the use of decay constants in geo and cosmochronology. *Earth Planet. Sci. Lett.* **1977**, *36*, 359–362. [[CrossRef](#)]
45. Wells, G.; Bryan, W.B.; Pearce, T.H. Comparative Morphology of Ancient and Modern Pillow Lavas. *J. Geol.* **1979**, *87*, 427–440. [[CrossRef](#)]
46. Ottens, B. Minerals of the Deccan Traps India. *Mineral. Rec.* **2003**, *34*, 5–83.
47. Subbarao, K.V. Sr isotopic evidence on the spilitic degradation of the Deccan basalt. *J. Earth Syst. Sci.* **2000**, *109*, 49–55. [[CrossRef](#)]
48. Frey, M.; De Capitani, C.; Liou, J.G. A new petrogenetic grid for low-grade metabasites. *J. Metamorph. Geol.* **1991**, *9*, 497–509. [[CrossRef](#)]
49. Coombs, D.; Ellis, A.; Fyfe, W.; Taylor, A. The zeolite facies, with comments on the interpretation of hydrothermal syntheses. *Geochim. Cosmochim. Acta* **1959**, *17*, 53–107. [[CrossRef](#)]
50. Kristmannsdottir, H. Alteration of Basaltic Rocks by Hydrothermal-Activity at 100–300 °C. *Dev. Sedimentol.* **1979**, *27*, 359–367. [[CrossRef](#)]
51. Cho, M.; Liou, J.G.; Maruyama, S. Transition from the Zeolite to Prehnite-Pumpellyite Facies in the Karmutsen Metabasites, Vancouver Island, British Columbia. *J. Pet.* **1986**, *27*, 467–494. [[CrossRef](#)]
52. Patil, R.R.; Panchapkesan, V.; Sahu, K.C. Fluid inclusions studies in amygdaloidal and vein Calcite in Deccan Traps. *Geol. Soc. India Mem.* **1981**, *3*, 422–427.
53. Rykart, R. *Quarz-Monographie*, 2nd ed.; Ott Verlag: Munich, Germany, 1995; 462p, ISBN 372256204X.
54. Currier, R. Bombay-Poona-Nasik. *Lapis* **1978**, *10*, 29–38.
55. Artioli, G.; Geiger, C.A.; Dapiaggi, M. The crystal chemistry of julgoldite-Fe³⁺ from Bombay, India, studied using synchrotron X-ray powder diffraction and ⁵⁷Fe Mössbauer spectroscopy. *Am. Mineral.* **2003**, *88*, 1084–1090. Available online: https://rruff-2.geo.arizona.edu/uploads/AM88_1084.pdf (accessed on 14 March 2022).
56. Nagashima, M.; Cametti, G.; Armbruster, T. Crystal chemistry of julgoldite, a mineral series of the pumpellyite group: Re-investigation of Fe distribution and hydrogen-bonding. *Eur. J. Mineral.* **2018**, *30*, 721–731. [[CrossRef](#)]
57. Weisenberger, T.; Bucher, K. Mass transfer and porosity evolution during low temperature water–rock interaction in gneisses of the simano nappe: Arvigo, Val Calanca, Swiss Alps. *Contrib. Mineral. Petrol.* **2011**, *162*, 61–81. [[CrossRef](#)]
58. Liou, J.G. Synthesis and stability relations of prehnite, Ca₂Al₂Si₃O₁₀(OH)₂. *Am. Mineral.* **1971**, *56*, 507–531.
59. Duggan, M.B. Babingtonite and Fe-rich Ca–Al silicates from western Southland, New Zealand. *Mineral. Mag.* **1986**, *50*, 657–665. [[CrossRef](#)]
60. Giret, A.; Verdier, O.; Nativel, P. The zeolitisation of Kerguelen Islands, Southern Indian Ocean. In *Recent Progress in Antarctic Earth Science*; Yoshida, Y., Ed.; Terra Publishing Co.: Tokyo, Japan, 1992; Volume 32, pp. 457–463.
61. Keith, T.E.C.; Staples, L.W. Zeolites in Eocene basaltic pillow lavas of the Siletz River volcanics, central coast range, Oregon. *Clays Clay Miner.* **1985**, *33*, 135–144. [[CrossRef](#)]

62. Barrer, R.M.; Marshall, D.J. Synthetic zeolites related to ferrierite and yugawaralite. *Am. Mineral.* **1965**, *50*, 484–489.
63. Seki, Y. Facies Series in Low-Grade Metamorphism. *J. Geol. Soc. Jpn.* **1969**, *75*, 255–266. [[CrossRef](#)]
64. Harada, K. Further Data on The Natural Association of Ca-Zeolites. *J. Geol. Soc. Jpn.* **1969**, *75*, 629–630. [[CrossRef](#)]
65. Zeng, Y.; Liou, J.G. Experimental investigation of yugawaralite wairakite equilibrium. *Am. Mineral.* **1982**, *67*, 937943.
66. Jørgensen, O. The regional distribution of zeolites in the basalts of the Faroe Islands and the significance of zeolites as palaeo-temperature indicators. *GEUS Bull.* **2006**, *9*, 123–156. [[CrossRef](#)]
67. Merlino, S. Gyrolite: Its Crystal Structure and Crystal Chemistry. *Mineral. Mag.* **1988**, *52*, 377–387. [[CrossRef](#)]
68. Lieber, W.; Arnold, R. Chemische Untersuchungen an „Poona“-Mineralien. *Lapis* **1984**, *5*, 28–29.
69. Ottens, B. *Indien, Mineralien und Fundstellen*; Weise: München, Germany, 2011; 384p, ISBN 10:3921656761.
70. Baltakys, K.; Siauciunas, R. Formation of gyrolite in the CaO–quartz–Na₂O–H₂O system. *Mater. Sci.* **2007**, *25*, 1089–1100.
71. Kurnosov, V.B.; Kholodkevich, I.V.; Shevchenko, A.Y. Secondary minerals of basalts from the Nauru Basin, Deep Sea Drilling Project, Leg 61. *Initial. Rep. Deep Sea Drill. Proj.* **1981**, *61*, 653–671.
72. Taylor, H.F.W. (Ed.) *The Chemistry of Cements*; Academic Press: Cambridge, MA, USA, 1964; Volume 1, 204p.
73. Dunn, P.J.; Rouse, R.C.; Norberg, J.A. Hydroxyapophyllite, a new mineral, and a redefinition of the apophyllite group; I, Description, occurrences, and nomenclature. *Am. Mineral.* **1978**, *63*, 196–199.
74. Rossmann, G.R. Optical spectroscopy of green vanadium apophyllite from Poona, India. *Am. Mineral.* **1974**, *59*, 621–622.
75. Srikantappa, C.; Mookherjee, A. Water, Aqueous, H₂O–CO₂ and Gaseous Inclusions in Cavity Minerals in the Basaltic Lava flows around Pune, India: Evidence for Boiling. In Proceedings of the Second Meeting of the Asian Current Research on Fluid Inclusions, (ACROFI–2) Issue, Kharagpur, India, 12–14 November 2008; Volume 176.
76. Weisenberger, T.B.; Rahn, M.; van der Lelij, R.; Spikings, R.A.; Bucher, K. Timing of low-temperature mineral formation during exhumation and cooling in the Central Alps, Switzerland. *Earth Planet. Sci. Lett.* **2012**, *327*, 1–8. [[CrossRef](#)]
77. Fleming, T.H.; Foland, K.A.; Elliot, D.H. Apophyllite⁴⁰Ar/³⁹Ar and Rb–Sr geochronology: Potential utility and application to the timing of secondary mineralization of the Kirkpatrick Basalt, Antarctica. *J. Geophys. Res. Earth Surf.* **1999**, *104*, 20081–20095. [[CrossRef](#)]
78. Molzahn, M.; Wörner, G.; Hejes-Kunst, F.; Rocholl, A. Constraints on the Cretaceous thermal event in the Transantarctic Mountains from alteration processes in Ferrar flood basalts. *Glob. Planet Change* **1999**, *23*, 45–60. [[CrossRef](#)]
79. Gebhard, G. Ferberit, ein neues Vorkommen aus den westindischen Basalten. *Lapis* **1994**, *19*, 41.
80. Arnórsson, S.; Óskarsson, N. Molybdenum and tungsten in volcanic rocks and in surface and <100 °C ground waters in Iceland. *Geochim. Cosmochim. Acta* **2007**, *71*, 284–304. [[CrossRef](#)]
81. Dill, H.G.; Füll, M.; Botz, R. Mineralogy and (economic) geology of zeolite-carbonate mineralization in basic igneous rocks of the Troodos Complex, Cyprus. *Neues Jahrbuch Für Mineralogie-Abhandlungen* **2007**, *183*, 251–268. [[CrossRef](#)]
82. Westercamp, D. Distribution and volcano-structural control of zeolites and other amygdale minerals in the Island of Martiniq, F.W.I. *J. Volcanol. Geotherm. Res.* **1981**, *11*, 353–365. [[CrossRef](#)]
83. Sethna, S.F.; Javeri, P. Geology and Petrochemistry of the Deccan Spilitic Basalts at and around Daman, India. *J. Geol. Soc. India* **1999**, *53*, 59–69.
84. Sultan, A. *A Photographic Atlas of Flood Basalt Volcanism*; Shet, H.C., Ed.; Springer International Publishing AG: Cham, Switzerland, 2018. [[CrossRef](#)]
85. Naik, A.; Sheth, H.; Samant, H.; D’Souza, S. Some observations on spilitized basalts of the western Deccan Traps, India. *Magmat. Earth Relat. Strateg. Met. Depos.* **2018**, *1*, 211–213.
86. Mookherjee, A.; Paradkar, M. Unusual Morphology of Laumontite clusters from near Soyaon, Aurangabad dist, Maharashtra, India. *J. Deccan Volcanol. Soc.* **2008**, *3–5*.
87. Lieber, W. Skolezith oder Mesolith oder Natrolith, Über die allzu großzügige Benennung indischer Zeolithe. *Lapis* **1996**, *6*, 13–16.
88. Götze, J.; Hofmann, B.; Machałowski, T.; Tsurkan, M.V.; Jesionowski, T.; Ehrlich, H.; Kleeberg, R.; Ottens, B. Biosignatures in Subsurface Filamentous Fabrics (SFF) from the Deccan Volcanic Province, India. *Minerals* **2020**, *10*, 540. [[CrossRef](#)]
89. Tschernich, R.W. *Zeolites of the World*; Geoscience Press: Phoenix, AZ, USA, 1992; 563p.
90. Faust, G. *A Review and Interpretation of the Geologic Setting of the Watchung Basalt Flows, New Jersey*; Professional Paper; U.S. Government Print Off.: Washington, DC, USA, 1975; 42p.
91. Mason, B.H. Trap rock minerals of New Jersey. *N. J. Geol. Surv. Bull.* **1960**, *64*, 1–51.
92. Laskowich, C.; Puffer, J.H. Prehnite and Zeolite distribution in the Orange Mountain Basalt Paterson, New Jersey. *Mineral. Rec.* **2016**, *47*, 479–490.